J. Fluid Mech. (2008), *vol.* 615, *pp.* 401–431.
doi:10.1017/S0022112008003807 Printed in the United Kingdom

Development of coherent structures in concentrated suspensions of swimming model micro-organisms

TAKUJI ISHIKAWA[1], J. T. LOCSEI[2] AND T. J. PEDLEY[2]

[1]Department of Bioengineering and Robotics, Tohoku University, 6-6-01, Aoba, Aramaki, Aoba-ku, Sendai 980-8579, Japan

[2]Department of Applied Mathematics and Theoretical Physics, University of Cambridge, Centre for Mathematical Sciences, Wilberforce Road, Cambridge CB3 0WA, UK

(Received 19 September 2007 and in revised form 27 July 2008)

A swimming micro-organism is modelled as a squirming sphere with prescribed tangential surface velocity and referred to as a squirmer. The centre of mass of the sphere may be displaced from the geometric centre, and the effects of inertia and Brownian motion are neglected. The well-known Stokesian dynamics method is modified in order to simulate squirmer motions in a concentrated suspension. The movement of 216 identical squirmers in a concentrated suspension without any imposed flow is simulated in a cubic domain with periodic boundary conditions, and the coherent structures within the suspension are investigated. The results show that (*a*) a weak aggregation of cells appears as a result of the hydrodynamic interaction between cells; (*b*) the cells generate collective motions by the hydrodynamic interaction between themselves; and (*c*) the range and duration of the collective motions depend on the volume fraction and the squirmers' stresslet strengths. These tendencies show good qualitative agreement with previous experiments.

1. Introduction

Continuum models for suspensions of swimming micro-organisms have been proposed for the analysis of phenomena such as bioconvection (Childress *et al.* 1975; Pedley & Kessler 1990; Hillesdon *et al.* 1995; Bees & Hill 1998; Metcalfe & Pedley 2001). The continuum models proposed so far are restricted to dilute suspensions, in which cell–cell interactions are negligible. In practice, however, one cannot assume diluteness for all suspensions of importance, such as the dense falling plumes that form part of bioconvection patterns (Kessler *et al.* 1994; Metcalfe & Pedley 2001), oceanic plankton blooms, harmful red tides in coastal regions, industrial bioreactors and so on. In order to deal with non-dilute suspensions of micro-organisms, it is necessary to consider the interactions between cells. Then the particle stress tensor, the velocities of the micro-organisms and the diffusion tensor in the continuum model will need to be replaced by improved expressions.

Dombrowski *et al.* (2004) have reported mesoscale coherent structures in a concentrated suspension of *Bacillus subtilis*. In a concentrated suspension, a *B. subtilis* cell apparently tends to swim in the same direction as its neighbours, generating a flow pattern larger than the scale of an individual cell but smaller than the scale of the container used in the experiment. The mesoscale structure changes its direction

randomly in a manner reminiscent of turbulence, so Dombrowski *et al.* named this phenomenon 'slow turbulence.' Mendelson *et al.* (1999) also observed a mesoscale motion of whorls and jets generated by *B. subtilis*. In this experiment, concentrated populations of *B. subtilis* are put on a thin water film above an agar gel. The collective motions dramatically change the trajectories of cells and the probability density function of the relative positions and orientations of the cells. Since coherent structures will affect the rheological and diffusive properties of a suspension, we will here numerically investigate the coherent structures that arise in a concentrated suspension of model cells, interacting purely hydrodynamically. One of the objectives of our work is to see whether hydrodynamics is enough to explain the coherent structures that arise in concentrated suspensions of swimmers, or whether some biological interaction must be postulated.

A significant amount of work has been done to analyse the micro-structure, or spatial distribution of particles, in concentrated suspensions of inert spheres, bubbles or droplets in a Stokes flow regime, because the micro-structure has a considerable influence on suspension rheology and diffusion, as found by Brady & Morris (1997) for a concentrated suspension of Brownian spheres in a simple shear flow. Acrivos (1995) investigated the self-diffusion of non-Brownian spheres in concentrated suspensions both experimentally and analytically. Though he explained three kinds of diffusive phenomena that may lead to aggregation of particles, strong aggregation was not observed in a suspension of uniform concentration under a constant applied shear rate. A concentrated suspension of deformable droplets has been investigated numerically by Loewenberg & Hinch (1996) and by Zinchenko & Davis (2000, 2002) in a vanishing Reynolds number (Re) regime. The suspension rheology is strongly affected by the micro-structure, but strong aggregation of droplets again has not been reported. Therefore, earlier research on the micro-structure of a suspension of inert particles cannot be simply extended to study that of active micro-organisms.

The model micro-organism used in this paper is the same as the one used by Ishikawa, Simmonds & Pedley (2006) and will be referred to as a 'squirmer'. Details of a squirmer will be briefly explained in § 2.1. The authors have already investigated the effect of cell–cell interaction on the rheology and self-diffusivity of a suspension of squirmers (Ishikawa & Pedley 2007*a*, *b*). The simulation methods employed in those studies are, however, restricted to 'semi-dilute' suspensions, because they are based on pairwise additivity in constructing the grand mobility matrix for the suspension as a whole. The error associated with this approximation in many-body interactions is $O(c^3)$ for the rheological properties, where c is the volume fraction of particles. Since an error $O(c^3)$ is not acceptable in the case of concentrated suspensions, it is necessary to improve the numerical method for such cases.

There are some methods that can efficiently simulate a concentrated suspension of particles, such as a lattice Boltzmann method (Ladd 1994*a*, *b*, 1997), a fast multipole method (Sangani & Mo 1996) and a modified boundary element method (Zinchenko & Davis 2000, 2002). The method to be used in this study is that of Stokesian dynamics, introduced by Brady & Bossis (1988). In the case of a spherical squirmer, the Faxén laws are simple (cf. equations (2.10)–(2.12)), so it is efficient to apply Stokesian dynamics to a suspension of squirmers. Details of the numerical method will be explained in § 2, and its reliability will be discussed in § 3 by comparison with available results.

In this paper, we will compute the three-dimensional motion of interacting squirmers in periodic suspensions in a fluid otherwise at rest. The coherent structures in a

suspension of squirmers will be investigated in § 4. Statistics of near-field interactions will be analysed in § 5. In § 6, we will compare the present numerical results with those of previous research, both experimental and numerical, and engage in further discussion.

2. Methods

The Stokesian dynamics simulation method for computing the hydrodynamic interactions among an infinite suspension of particles, in the absence of Brownian motion and at negligible particle Reynolds number, was developed by Brady *et al.* (1988). This method was extended by Mehandia & Nott (2007) for dipole spheres. The numerical method used in this study is similar to theirs, but it had to be modified in order to deal with squirmers instead of inert spheres. To our knowledge, Brady's Stokesian dynamics method has not previously been exploited for squirmers, so we explain the modified method in detail in this section. (Of course, dynamic simulations of active particles in Stokes flow have been reported but without accurate representation of the near field.)

2.1. *A squirmer*

The model micro-organism used in this paper (a spherical squirmer) is the same as the one used by Ishikawa *et al.* (2006). It is assumed to be neutrally buoyant (i.e. force-free), possibly bottom-heavy (therefore not necessarily torque-free) and non-Brownian, and it is also assumed to swim at very small Reynolds number; i.e. it is assumed to be inertia-free. The model of a squirmer was first proposed by Lighthill (1952), and has been extended by Blake (1971), Felderhof & Jones (1994) and Stone & Samuel (1996). The model has also been used by Magar, Goto & Pedley (2003) and Magar & Pedley (2005) to analyse nutrient uptake properties of a solitary squirmer.

The sphere's surface is assumed to move purely tangentially, and these tangential motions are assumed to be axisymmetric and time-independent. Thus the tangential surface velocity of a squirmer, in the reference frame moving along with the squirmer, is given as

$$\boldsymbol{u}_s = \sum_{n=1}^{2} \frac{2}{n(n+1)} B_n \left(\frac{\boldsymbol{e}\cdot\boldsymbol{r}}{r}\frac{\boldsymbol{r}}{r} - \boldsymbol{e} \right) P_n'(\boldsymbol{e}\cdot\boldsymbol{r}/r), \tag{2.1}$$

where P_n is the nth Legendre polynomial, $\boldsymbol{e}$ is the unit orientation vector of a squirmer, $\boldsymbol{r}$ is the position vector and $r = |\boldsymbol{r}|$. We will follow Ishikawa *et al.* (2006) and omit squirming modes higher than the second (i.e. $B_n = 0$ in $\boldsymbol{u}_s$ when $n \geqslant 3$), though such a restriction is not required for the numerical methods to work. The swimming speed of a solitary squirmer is $U_{sol} = 2B_1/3$. We denote by β the ratio of second-mode squirming to first-mode squirming; i.e. $\beta = B_2/B_1$. It should be noted that B_2, and hence β, can have either sign. A squirmer with positive β is a 'puller', analogous to a micro-organism for which the thrust-generating apparatus is in front of the body (which dominates the drag), as in biflagellate algae such as *Chlamydomonas*, whereas a squirmer with negative β is a 'pusher'; i.e. the thrust is generated behind the body, as in bacteria or spermatozoa. In the present study, we intend to discuss coherent structures in a general suspension of active particles whose hydrodynamics can be modelled precisely. Thus we do not use a bacterium-specific model (as did Ishikawa *et al.* 2007), even though coherent structures are often discussed in a bacterial bath. Ishikawa & Hota (2006) experimentally showed that the squirmer is a good model for one kind of ciliated protozoan, *Paramecium*, and there are other real micro-organisms,

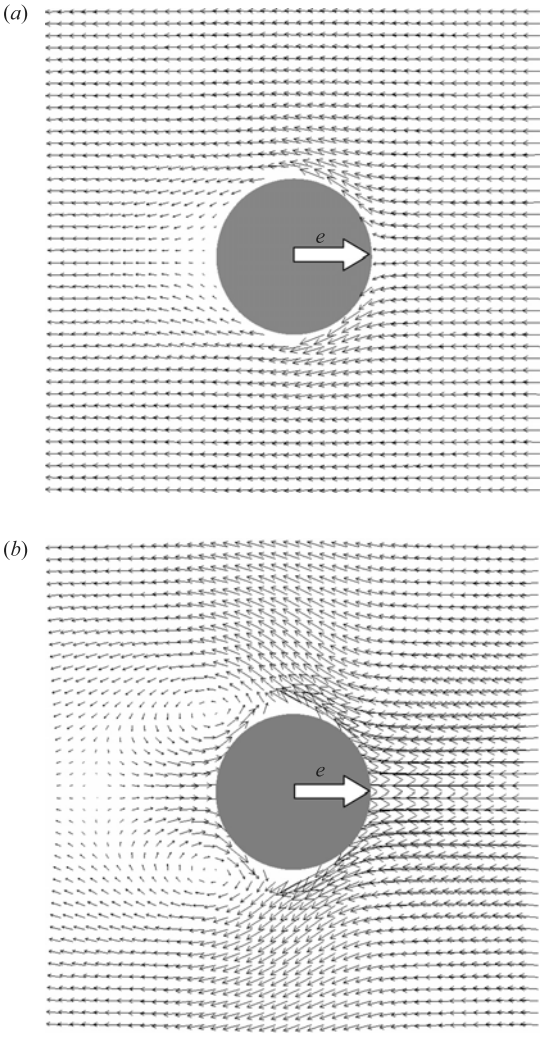

FIGURE 1. Velocity vectors in the reference frame moving along with the squirmer. Uniform flow of speed 1, in dimension-free form, coming from far right. The scales of vectors in (*a*) and (*b*) are the same. (*a*) $\beta = 1$; (*b*) $\beta = 5$.

notably ciliates such as *Opalina* and colonies of flagellates such as *Volvox*, which may be modelled as squirmers. Moreover, cyanobacteria (Waterbury *et al.* 1985) also have no external appendages, and they swim by a bulk streaming of the cell surface without observable shape change (Pitta & Berg 1995). Thus, they may be modelled as squirmers, too. However, it should be emphasized that our choice of a spherical squirmer as a model micro-organism was made because it was the simplest we could think of that also permitted a precise analysis of the hydrodynamics, even in the near field (Ishikawa *et al.* 2006). By treating the fluid dynamics precisely we can be sure that any emergent behaviours really do emerge as consequences of hydrodynamical interactions and not as artefacts of a near-field approximation scheme. Velocity vectors, relative to the translational velocity vector of a squirmer, for the cases $\beta = 1$ and 5 are explicitly shown in figure 1.

There have been some previous investigations of the hydrodynamic interactions between micro-organisms (Guell *et al.* 1988; Ramia, Tullock & Phan-Thien 1993; Nasseri & Phan-Thien 1997; Jiang, Osborn & Meneveau 2002; Lega & Passot 2003; Hernandes-Ortiz, Stoltz & Graham 2005; Saintillan & Shelley 2007), but none of them has studied micro-organisms in near contact. Apart from the last of these papers, the dependence of coherent structures on the details of the micro-organisms' interactions has also not been discussed before. Recently, the trajectories of real interacting micro-organisms (modelled as spheroidal squirmers) were experimentally and computationally investigated by Ishikawa & Hota (2006); their results show that the interaction is indeed mainly hydrodynamic and that the squirmer model is a good one.

2.2. *Multipole expansion*

Isothermal Stokes flow of an incompressible Newtonian fluid is considered. When N squirmers are periodically replicated in three-dimensional space, the governing equation of the flow field external to the squirmers can be given in integral form, using the single-layer potential only, as

$$u_i(\boldsymbol{x}) - \langle u_i(\boldsymbol{x})\rangle = -\frac{1}{8\pi\mu}\sum_{\alpha=1}^{N}\int_{A_\alpha} J_{ij}(\boldsymbol{x}-\boldsymbol{y})q_j(\boldsymbol{y})\,\mathrm{d}A_y, \tag{2.2}$$

where $\boldsymbol{u}$ is the velocity, $\boldsymbol{q}$ is the single-layer potential and A is the surface of a particle (see Pozrikidis 1992). $\boldsymbol{J}$ is the Green function for a triply periodic lattice, which is evaluated by Ewald summation on the lattice and reciprocal lattice of image points, as explained by Beenakker (1986). The brackets $\langle\rangle$ indicate the suspension average. The single-layer potential, $\boldsymbol{q}$, is the difference between the traction force on the inner surface, $\boldsymbol{f}_{in}$, and that on the outer surface, $\boldsymbol{f}_{out}$, given by

$$\boldsymbol{q} = \boldsymbol{f}_{out} - \boldsymbol{f}_{in}. \tag{2.3}$$

The velocity field generated by point forces in a homogeneous fluid is expressed by (2.2) with the boundary condition (2.1). So it also induces an axisymmetric flow field inside the spheres, which make $\boldsymbol{f}_{in}$ non-zero. In order to impose a rigid-body motion inside the spheres, one needs to introduce a double-layer potential in (2.2) and to deal with velocity slip on the surface explicitly. Introducing double-layer potentials, however, makes the multipole expansion much more tedious and considerably increases the computational load. Since $\boldsymbol{f}_{in}$ can be obtained analytically in the case of a squirmer, it is computationally more efficient to express the velocity field in terms of single-layer potentials only than by using two kinds of potential. The effect of $\boldsymbol{f}_{in}$ appears in calculating the stresslet strength of a squirmer, so it is subtracted analytically as will be explained later on. The boundary element method using single- or double-layer potentials only, a so-called generalized boundary integral method, is explained in detail, including the derivation of integral equations and the force and torque exerted on a particle, in an established text by Pozrikidis (1992).

The right-hand side of (2.2) can be expanded in moments about the centre of each particle with radius a as (see Durlofsky, Brady & Bossis 1987)

$$u_i(\boldsymbol{x}) - \langle u_i(\boldsymbol{x})\rangle = \frac{1}{8\pi\mu}\sum_{\alpha=1}^{N}\left[\left(1+\frac{a^2}{6}\nabla^2\right)J_{ij}F_j^\alpha + R_{ij}L_j^\alpha + \left(1+\frac{a^2}{10}\nabla^2\right)K_{ijk}S_{jk}^\alpha + \nabla_k\nabla_l J_{ij}Q_{klj}^\alpha + \cdots\right], \tag{2.4}$$

where $\boldsymbol{F}, \boldsymbol{L}, \boldsymbol{S}, \boldsymbol{Q}$ are respectively the monopole, the antisymmetric dipole, the symmetric dipole, the irreducible quadrupole of the single-layer potential. The propagators are given as follows:

$$R_{ij} = \epsilon_{lkj}\frac{1}{4}(\nabla_k J_{il} - \nabla_l J_{ik}), \quad K_{ijk} = \frac{1}{2}(\nabla_k J_{ij} + \nabla_j J_{ik}), \tag{2.5}$$

where $\boldsymbol{\epsilon}$ is the unit-alternating isotropic tensor.

There is no contribution of $\boldsymbol{f}_{in}$ to the force and torque; therefore the force and torque exerted on the fluid are analogous to the monopole $\boldsymbol{F}$ and the antisymmetric dipole $\boldsymbol{L}$ of the single-layer potential, respectively (Pozrikidis 1992). The force and torque a squirmer exerts on the fluid are given by

$$\boldsymbol{F}^\alpha = -\int_{A_\alpha} \boldsymbol{q}(\boldsymbol{x})\,\mathrm{d}A_x, \quad \boldsymbol{L}^\alpha = -\int_{A_\alpha} \boldsymbol{x}\wedge\boldsymbol{q}(\boldsymbol{x})\,\mathrm{d}A_x. \tag{2.6}$$

However, $\boldsymbol{f}_{in}$, does contribute to the stresslet, and one needs to calculate it carefully. The stresslet, $\hat{\boldsymbol{S}}$, a squirmer exerts on the fluid can be expressed as (see Batchelor 1970)

$$\hat{\boldsymbol{S}}^\alpha = -\int_{S_\alpha}\left[\frac{1}{2}\{\boldsymbol{f}_{out}\boldsymbol{x} + \boldsymbol{x}\boldsymbol{f}_{out}\} - \frac{1}{3}\boldsymbol{x}\cdot\boldsymbol{f}_{out}\boldsymbol{I} - \mu(\boldsymbol{u}\boldsymbol{n} + \boldsymbol{n}\boldsymbol{u})\right]\mathrm{d}S_x, \tag{2.7}$$

where $\boldsymbol{n}$ is the outward normal vector, and $\boldsymbol{I}$ is the unit tensor. In the case of a squirmer, the last term in the right-hand side of (2.7) can be expressed in terms of $\boldsymbol{f}_{in}$ (detailed derivation in Appendix B of Ishikawa *et al.* 2006), and $\hat{\boldsymbol{S}}$ can be expressed by the single-layer potential as

$$\hat{\boldsymbol{S}}^\alpha = -\int_{S_\alpha}\left[\frac{1}{2}(\boldsymbol{q}\boldsymbol{x} + \boldsymbol{x}\boldsymbol{q}) - \frac{1}{3}\boldsymbol{x}\cdot\boldsymbol{q}\boldsymbol{I}\right]\mathrm{d}S_x = \boldsymbol{S}^\alpha. \tag{2.8}$$

Thus the stresslet $\hat{\boldsymbol{S}}$ is also analogous to the symmetric dipole $\boldsymbol{S}$ of the single-layer potential.

The irreducible quadrupole, $\boldsymbol{Q}$, that a squirmer exerts on the fluid, is defined by

$$Q^\alpha_{klj} = -\frac{1}{2}\int_{A_\alpha}\left(y_k - x^\alpha_k\right)\left(y_l - x^\alpha_l\right)q_j\mathrm{d}A_y - \frac{a^2}{6}F^\alpha_j\delta_{kl}, \tag{2.9}$$

where $\boldsymbol{x}^\alpha$ is the centre of particle α.

2.3. *Formation of the grand mobility matrix*

In order to determine the motion of a squirmer in the flow field given by (2.2), we exploit the Faxén laws for a squirmer. The Faxén laws for the force, torque and stresslet for a squirmer can be found in Ishikawa *et al.* (2006):

$$U^\alpha_i - \langle u_i(\boldsymbol{x}^\alpha)\rangle = \frac{F^\alpha_i}{6\pi\mu a} + \frac{2}{3}B^\alpha_1 e^\alpha_i + \left(1 + \frac{a^2}{6}\nabla^2\right)u'_i(\boldsymbol{x}^\alpha), \tag{2.10}$$

$$\Omega^\alpha_i - \langle\omega_i(\boldsymbol{x}^\alpha)\rangle = \frac{L^\alpha_i}{8\pi\mu a^3} + \frac{1}{2}\epsilon_{ijk}\nabla_j u'_k(\boldsymbol{x}^\alpha), \tag{2.11}$$

$$\begin{aligned}-\langle E_{ij}(\boldsymbol{x}^\alpha)\rangle = {}& \frac{S^\alpha_{ij}}{\frac{20}{3}\pi\mu a^3} + \frac{1}{5}\mu a^2 B^\alpha_2\left(3e^\alpha_i e^\alpha_j - \delta_{ij}\right)\\ & + \frac{1}{2}\left(1 + \frac{a^2}{10}\nabla^2\right)(\nabla_j u'_i(\boldsymbol{x}^\alpha) + \nabla_i u'_j(\boldsymbol{x}^\alpha)),\end{aligned} \tag{2.12}$$

where $\boldsymbol{U}$ and $\boldsymbol{\Omega}$ are the translational and rotational velocities of the squirmer, respectively, $\langle\boldsymbol{\omega}\rangle$ is the angular velocity of the bulk suspension $\langle\boldsymbol{E}\rangle$ is the rate of strain tensor of the bulk suspension and $\boldsymbol{u}'$ is the disturbance velocity field caused by the other particles. Since a solitary squirmer swims with a constant velocity, an additional second term appears on the right-hand side of (2.10). A solitary squirmer also generates a stresslet (see Ishikawa *et al.* 2006), so the second term appears on the right-hand side of (2.12).

The velocity disturbance caused by a stresslet decays as r^{-2}, while the next moment, a quadrupole, creates a disturbance that decays as r^{-3}. By integrating over an infinite volume, one can show that the effect of a quadrupole is marginally important compared with that of a stresslet. The next moment, an octupole, creates a disturbance that decays as r^{-4}, so the velocity disturbance caused by octupoles and higher moments vanishes after integration over an infinite volume of the suspension. The quadrupole of a squirmer may be derived from (2.28) in Brady *et al.* (1988) as

$$Q^{\alpha}_{klj} = \left(\frac{a^2}{10}c\langle F_m\rangle + 2\pi\mu a^3 B_1^{\alpha} e_m^{\alpha}\right)\left(\delta_{km}\delta_{jl} + \delta_{lm}\delta_{kj} - \frac{2}{3}\delta_{kl}\delta_{jm}\right) + \frac{3a^3}{4}\sum_{i\neq\alpha}\int_{A_i} G_{kl}J_{jm}q_m \,\mathrm{d}A + \frac{9c}{16\pi}\int_V G_{kl}J_{jm}\langle F_m\rangle \,\mathrm{d}V, \tag{2.13}$$

where c is the volume fraction of particles, and V is the volume for suspension averaging. $G_{kl}J_{jm}$ is a second-order differential operator, but the detailed form is not needed here. Since a solitary squirmer generates a quadrupole, an additional term with B_1^{α} appears on the right-hand side of (2.13). We will follow Brady *et al.* (1988) and neglect the last two integrals on the right-hand side of (2.13), in order to reduce the computational load. Brady *et al.* concluded that the additional accuracy provided by retaining the full quadrupole expression (2.13) is not worth the additional computational costs. Thus we will calculate as far as the stresslet in the multipole expansion given by (2.4), and the quadrupole will be approximated by (2.13) without the last two integrals.

The convergent expressions for squirmer interactions in a fluid suspension can be derived by substituting $\boldsymbol{u} - \langle\boldsymbol{u}\rangle$ in the multipole expansion given by (2.4) for $\boldsymbol{u}'$ in (2.10)–(2.12). The result is expressed in matrix form as

$$\begin{pmatrix} \boldsymbol{U} - \langle\boldsymbol{u}\rangle - \frac{2}{3}B_1\boldsymbol{e} + \boldsymbol{Q}_{sq} \\ \boldsymbol{\Omega} - \langle\boldsymbol{\omega}\rangle \\ -\langle\boldsymbol{E}\rangle - \frac{1}{5}B_2(3\boldsymbol{ee} - \boldsymbol{I}) \end{pmatrix} = \boldsymbol{M}^{far}\begin{pmatrix} \boldsymbol{F} \\ \boldsymbol{L} \\ \boldsymbol{S} \end{pmatrix}, \tag{2.14}$$

where $\boldsymbol{Q}_{sq}$ is given by

$$Q^{\alpha}_{sq,i} = \frac{1}{8\pi\mu}\sum_{n}^{N\prime}\frac{4\pi a^2}{3}B_1^n\nabla^2 J_{ij}e_j^n. \tag{2.15}$$

The prime on the sum indicates that the $n=\alpha$ term is excluded from the Ewald summation. $\boldsymbol{M}^{far}$ is the grand mobility matrix, which is equal to the one derived by Brady *et al.* (1988) for a suspension of inert spheres. The effect of the

squirming motion appears only on the left-hand side of (2.14). We should note that $\boldsymbol{M}^{far}$ is symmetric and positive definite. In order to satisfy positive definiteness, the integration in (2.2) needs to be performed over an infinite volume of the suspension.

2.4. *Inclusion of near-field interactions*

The inverse of the grand mobility matrix $\boldsymbol{M}^{far}$ is the grand resistance matrix $\boldsymbol{R}^{far}$. As discussed by Durlofsky *et al.* (1987), inverting the Ewald-summed mobility matrix sums an infinite number of reflected interactions among an infinite number of particles. In an earlier work, we have used the grand resistance matrix based on pairwise additivity, which is applicable only to a semi-dilute regime (Ishikawa & Pedley 2007*a*, *b*). The grand resistance matrix constructed here, on the other hand, is applicable to any volume fraction of particles, because inverting the mobility matrix is a true many-body approximation to the resistance matrix. The error in the grand resistance matrix is no longer $O(c^3)$. $\boldsymbol{R}^{far}$ still lacks, however, near-field interactions, because they are reproduced only when all multipoles are included. In order to include the near-field interactions, we will follow the method of Durlofsky *et al.* and add near-field multipoles in a pairwise additive fashion. Durlofsky *et al.* showed that the following procedure of including lubrication is remarkably accurate for any configuration of a finite number of particles.

When the minimum separation between two squirmer surfaces is small enough, i.e. less than $0.1a$ in this study, we add the force $\boldsymbol{F}^{near}$, torque $\boldsymbol{L}^{near}$ and stresslet $\boldsymbol{S}^{near}$ generated by pairs of squirmers. By exploiting the linearity of the flow field, near-field multipoles can be divided into two simpler multipoles: (*a*) the multipoles generated by two inert spheres with translational and rotational velocities in a linear flow field and (*b*) the multipoles generated by two squirmers without translational and rotational velocities in a fluid otherwise at rest. Thus $\boldsymbol{F}^{near}$, $\boldsymbol{L}^{near}$ and $\boldsymbol{S}^{near}$ can be expressed as

$$\begin{pmatrix} \boldsymbol{F}^{near} \\ \boldsymbol{L}^{near} \\ \boldsymbol{S}^{near} \end{pmatrix} = \boldsymbol{R}_{2B}^{near} \begin{pmatrix} \boldsymbol{U} - \langle \boldsymbol{u} \rangle \\ \boldsymbol{\Omega} - \langle \boldsymbol{\omega} \rangle \\ -\langle \boldsymbol{E} \rangle \end{pmatrix} + \begin{pmatrix} \boldsymbol{F}_{sq}^{near} \\ \boldsymbol{L}_{sq}^{near} \\ \boldsymbol{S}_{sq}^{near} \end{pmatrix}, \tag{2.16}$$

where $\boldsymbol{R}_{2B}^{near}$ is the exact two-sphere resistance matrix, which can be found in Kim & Karrila (1992), for instance. $\boldsymbol{F}_{sq}^{near}$, $\boldsymbol{L}_{sq}^{near}$ and $\boldsymbol{S}_{sq}^{near}$ are respectively the force, torque and stresslet generated by two squirmers without translational and rotational velocities in a fluid otherwise at rest. We have already compiled a database of pairwise interactions of squirmers (Ishikawa *et al.* 2006), so we will use the database in constructing these multipoles.

Part of the two-squirmer resistance interaction, the far-field part, has already been included upon the inversion of $\boldsymbol{M}^{far}$, so we have to subtract it off. The matrix composed of these two-body infinite reflection interactions is denoted by $\boldsymbol{R}_{2B}^{far}$. Finally, the complete expressions for squirmer interactions in a fluid suspension can be given as

$$\begin{pmatrix} \boldsymbol{F} \\ \boldsymbol{L} \\ \boldsymbol{S} \end{pmatrix} = \left[\boldsymbol{R}^{far} - \boldsymbol{R}_{2B}^{far}\right] \begin{pmatrix} \boldsymbol{U} - \langle \boldsymbol{u} \rangle - \frac{2}{3} B_1 \boldsymbol{e} + \boldsymbol{Q}_{sq} \\ \boldsymbol{\Omega} - \langle \boldsymbol{\omega} \rangle \\ -\langle \boldsymbol{E} \rangle - \frac{1}{5} B_2 (3\boldsymbol{e}\boldsymbol{e} - \boldsymbol{I}) \end{pmatrix} + \begin{pmatrix} \boldsymbol{F}^{near} \\ \boldsymbol{L}^{near} \\ \boldsymbol{S}^{near} \end{pmatrix}. \tag{2.17}$$

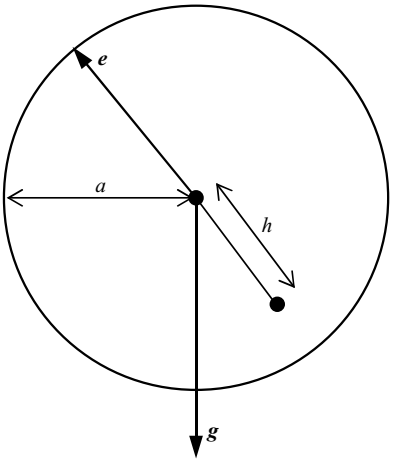

FIGURE 2. A sketch of the arrangement of a bottom-heavy squirmer. Gravity acts in the $\boldsymbol{g}$ direction, while the squirmer has orientation vector $\boldsymbol{e}$ and radius a, and its centre of mass is at distance h from its geometrical centre.

The unknown quantities in this equation are $\boldsymbol{U}$, $\boldsymbol{\Omega}$ and $\boldsymbol{S}$. This equation can be rewritten as

$$\begin{pmatrix} \boldsymbol{F} \\ \boldsymbol{L} \\ \boldsymbol{S} \end{pmatrix} = \left[\boldsymbol{R}^{far} - \boldsymbol{R}^{far}_{2B} + \boldsymbol{R}^{near}_{2B}\right] \begin{pmatrix} \boldsymbol{U} - \langle \boldsymbol{u} \rangle \\ \boldsymbol{\Omega} - \langle \boldsymbol{\omega} \rangle \\ -\langle \boldsymbol{E} \rangle \end{pmatrix} + \left[\boldsymbol{R}^{far} - \boldsymbol{R}^{far}_{2B}\right] \begin{pmatrix} -\frac{2}{3} B_1 \boldsymbol{e} + \boldsymbol{Q}_{sq} \\ 0 \\ -\frac{1}{5} B_2 (3\boldsymbol{ee} - \boldsymbol{I}) \end{pmatrix} + \begin{pmatrix} \boldsymbol{F}^{near}_{sq} \\ \boldsymbol{L}^{near}_{sq} \\ \boldsymbol{S}^{near}_{sq} \end{pmatrix}. \tag{2.18}$$

The first matrix multiplication on the right-hand side of (2.18) indicates the contribution from two inert spheres with translational and rotational velocities in a linear flow field, which is equal to the equation derived by Brady *et al.* (1988). The second matrix multiplication indicates the far-field contribution from the squirming motion, and the last term indicates the near-field contribution from the squirming motion.

2.5. *A gravitational torque and a repulsive force*

If squirmers are bottom-heavy, external gravitational torques are generated when they are not vertically oriented, and they tend to swim upwards on average. The fact that micro-organisms are generally somewhat denser than water, and therefore experience a net gravitational force, is neglected in this study because the sedimentation speed of dead cells is much less than the swimming speed of live cells (Kessler 1986). If the distance of the centre of mass is h from the centre of the squirmer, in the direction opposite to its swimming direction in undisturbed fluid (see figure 2), then there is an additional torque of

$$\boldsymbol{L}_{bh} = \frac{4}{3}\pi a^3 \rho h \boldsymbol{e} \wedge \boldsymbol{g}, \tag{2.19}$$

where ρ is the cell density; $\boldsymbol{g}$ is the gravitational acceleration vector; and the gravitational direction is $\boldsymbol{g}/g$.

A non-hydrodynamic inter-particle repulsive force $\boldsymbol{F}_{rep}$ is added to the system in order to avoid the prohibitively small time step needed to overcome the problem of overlapping particles. We will follow Brady & Bossis (1985) and Ishikawa & Pedley (2007*a*), and use the following function:

$$\boldsymbol{F}_{rep} = \alpha_1 \frac{\alpha_2 \exp(-\alpha_2 \varepsilon)}{1 - \exp(-\alpha_2 \varepsilon)} \frac{\boldsymbol{r}}{r}, \tag{2.20}$$

where α_1 is a dimensional coefficient; α_2 is a dimensionless coefficient; and ε is the minimum separation between squirmer surfaces non-dimensionalized by their radius. The coefficients used in this study are $\alpha_1 = 1$ and $\alpha_2 = 10^3$. The minimum separation obtained with these parameters is between 10^{-3} and 10^{-4}, compared with the separation of 10^{-1} below which the near-field lubrication forces have to be treated explicitly. The effect of the repulsive force on the trajectories of cells is very small, because it acts only in the very near field and changes the distance between particles by only around 10^{-4}.

2.6. *Numerical methods*

We will calculate interacting squirmers' motion in a fluid otherwise at rest ($\langle \boldsymbol{E} \rangle = \boldsymbol{0}$). The computational region is a cube with side H. A suspension of infinite extent is modelled by applying periodic boundary conditions, and the interactions among an infinite number of particles are calculated by the Ewald summation over the next two layers from the unit cell on the real- and reciprocal-space lattices. The convergence parameter in the Ewald sum is set at the optimal value $\sqrt{\pi}/H$ (Beenakker 1986), and the sum converges extremely rapidly. The time marching is performed by the fourth-order Adams–Bashforth scheme, for random initial positions and orientations. Although we have used a particle number N that ranges up to 216, it is not large enough for the scale of the coherent structures to be completely independent of it. The effect of particle number will be explicitly discussed later on in § 4 (cf. figure 11). Fortunately, the particle number does not affect the results qualitatively in the range used in this study, and we see a number of phenomena that have been observed in experiments emerge (cf. § 6).

All equations are non-dimensionalized using the radius a, characteristic velocity $U_{sol} = 2B_1/3$ and the fluid viscosity μ. There is one important dimensionless parameter in addition to β and c, G_{bh}, which is proportional to the ratio of the time to swim a body length to the time to rotate to face up and is defined as

$$G_{bh} = \frac{2\pi \rho g a h}{\mu B_1}. \tag{2.21}$$

3. Benchmark tests for the present numerical methods

Since exact solutions for a concentrated suspension of squirmers have not previously been reported, we check the reliability of the present numerical methods by comparison with (*a*) the exact solution for a concentrated suspension consisting of a simple cubic array of spheres, (*b*) numerical results for two-squirmer interactions obtained by the boundary integral method and (*c*) numerical results for a semi-dilute suspension of squirmers obtained by a Stokesian dynamics simulation, in which the grand resistance matrix is constructed in a pairwise additive manner. In comparison (*a*), the accuracy of the final form of the grand resistance matrix, $[\boldsymbol{R}^{far} - \boldsymbol{R}^{far}_{2B} + \boldsymbol{R}^{near}_{2B}]$, in (2.18) can be checked. In comparisons (*b*) and (*c*), the accuracy

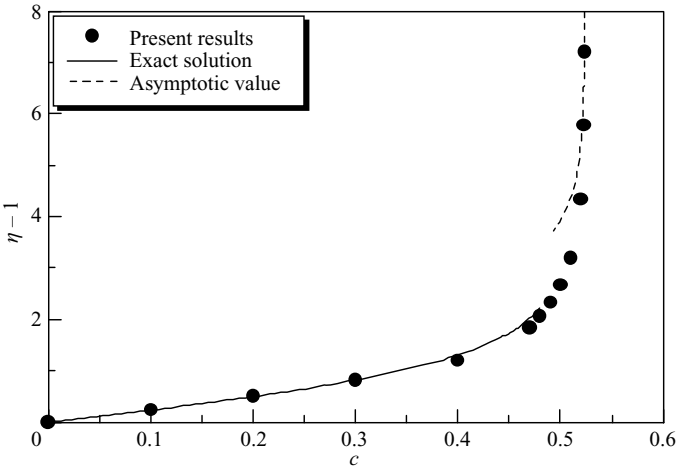

FIGURE 3. The shear viscosity of an infinite suspension of a simple cubic array of spheres as a function of volume fraction. The exact solution is obtained by Nunan & Keller (1984), and the asymptotic value is calculated by (3.1).

of the last two terms on the right-hand side of (2.18) can be checked in a semi-dilute regime.

3.1. *A concentrated suspension of spheres in a simple cubic array*

The accuracy of the grand resistance matrix in (2.18) has already been discussed in Brady *et al.* (1988). Similar results will be shown here, but we will explain them again in order to help readers assess the accuracy of our computation.

The apparent shear viscosity, η, of an infinite suspension, consisting of a simple cubic array of spheres, is calculated by the present methods (with η being non-dimensionalized by μ). The results are shown in figure 3, in which the exact solutions up to $c = 0.48$ and the asymptotic values, both obtained by Nunan & Keller (1984), are shown as well. The asymptotic equation is given by

$$\eta - 1 = \frac{\pi}{4} \ln \epsilon^{-1} + 0.63, \quad \text{where} \quad \epsilon = 1 - \left(\frac{6c}{\pi}\right)^{1/3}. \tag{3.1}$$

We see that the present results agree well with the exact solution in the range $0 \leqslant c \leqslant 0.48$. The agreement in the $c \ll 1$ regime indicates that the propagators for the force, torque and stresslet in the far-field separation, $\boldsymbol{M}^{far}$ in (2.14), are correctly modelled by the present method. The present results show singular behaviour when c approaches $\pi/6$, which is the value obtained from the asymptotic analysis by Nunan & Keller (1984). The asymptotic behaviour is dominated by the lubrication forces between spheres, so it is confirmed that the present method can correctly describe the lubrication forces as well. Consequently, the near-field and far-field interactions between an infinite number of spheres are correctly described by the present method over the whole range of c.

We have also calculated the sedimentation velocity of a simple cubic array of spheres. The results were compared with table 1 in Brady *et al.* (1988), and the difference between the two results was less than 1 % when $0.001 \leqslant c \leqslant 0.5236$.

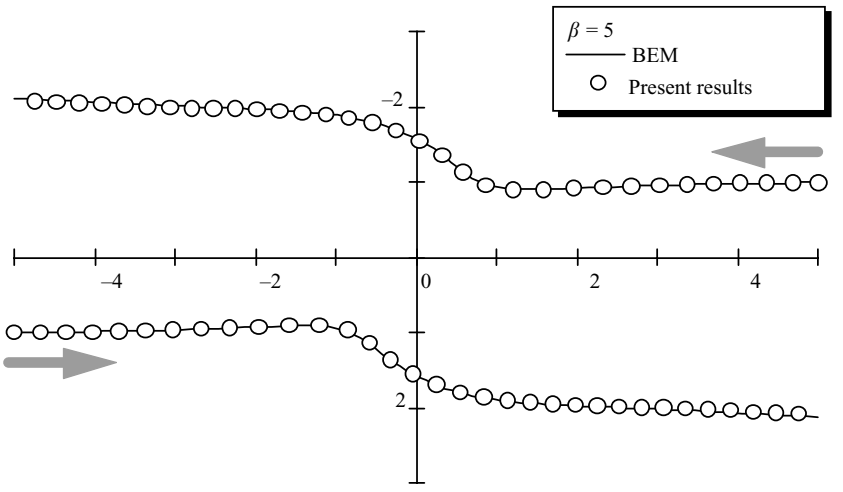

FIGURE 4. Comparison of two-squirmer trajectories obtained by the present method and the boundary element method (BEM). Two squirmers with $\beta = 5$ are facing each other initially, and the arrows in the figure show the directions of the trajectories.

3.2. *Two-squirmer interaction*

In this section, we will discuss whether the interaction due to squirming can be correctly described by the last two terms in (2.18). The far-field interaction due to squirming motion is given by the second term on the right-hand side of (2.18), whereas the near-field interaction is given by the last term. The resistance matrix $[\boldsymbol{R}^{far} - \boldsymbol{R}^{far}_{2B}]$ in the second term is included in the final form of the grand resistance matrix, $[\boldsymbol{R}^{far} - \boldsymbol{R}^{far}_{2B} + \boldsymbol{R}^{near}_{2B}]$, whose accuracy was checked in the previous section.

The trajectories of two squirmers initially swimming in opposite directions on slightly offset paths are shown in figure 4 ($\beta = 5$). The arrows in the figure show the directions of the trajectories. The solid lines in the figure are obtained by the full boundary integral method (Ishikawa *et al.* 2006), and the circles are obtained by the present method. We see that the two squirmers come close to each other, then change their orientation in the near field and finally avoid each other. The two trajectories match perfectly, which indicates that the translational and rotational velocities of two interacting squirmers can be correctly described by (2.18). We have also compared the time change of the stresslet in this case, and the results show good agreement. We have tried some other cases such as (*a*) two-squirmer interaction with different initial conditions, (*b*) interaction of two bottom-heavy squirmers and (*c*) two-squirmer interaction under a simple shear flow. All of these results show excellent agreement, though they are omitted here.

3.3. *A semi-dilute suspension of squirmers*

The translational cell diffusivity is a measure of the increasing displacements between pairs of particles. Thus one calculates the mean square displacement, which necessarily grows with time. If it grows more rapidly than linearly in time, then the spread is not diffusive (if proportional to t^2, it is as if the relative velocity of two spheres were constant), but if it becomes linear in time, then the spread is diffusive. Since we do not know whether the spreading is diffusive or not, we define a translational cell

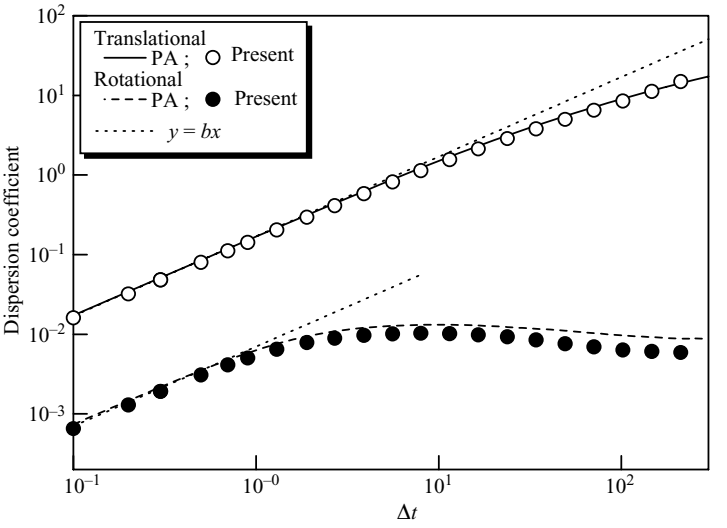

FIGURE 5. Comparison of dispersion coefficient between two methods ($c = 0.1$, $\beta = 1$ and $G_{bh} = 0$). The present method using 64 squirmers is indicated by *present*, and *PA* indicates the former results using 27 squirmers in which the grand mobility matrix is constructed in a pairwise additive manner. The function $y = bx$, where b is a coefficient, is drawn as well for comparison.

dispersion tensor, $\boldsymbol{D}^T$, by dividing the mean square displacement by time:

$$\boldsymbol{D}^T(\Delta t) = \frac{\langle [\boldsymbol{r}(t+\Delta t) - \boldsymbol{r}(t)][\boldsymbol{r}(t+\Delta t) - \boldsymbol{r}(t)] \rangle}{2\Delta t}, \tag{3.2}$$

where $\boldsymbol{r}$ is the translational displacement. If $\boldsymbol{D}^T$ asymptotes to a constant value as $\Delta t \to \infty$, the asymptotic value is the diffusion coefficient. A similar calculation is carried out for angular displacement, leading to the rotational cell dispersion tensor $\boldsymbol{D}^R$:

$$\boldsymbol{D}^R(\Delta t) = \frac{\langle [\boldsymbol{\lambda}(t+\Delta t) - \boldsymbol{\lambda}(t)]\,[\boldsymbol{\lambda}(t+\Delta t) - \boldsymbol{\lambda}(t)] \rangle}{2\Delta t}, \tag{3.3}$$

where $\boldsymbol{\lambda}$ is the rotational displacement. The dispersion of squirmers in a semi-dilute suspension was investigated by Ishikawa & Pedley (2007*b*); 'semi-dilute' here means that most of the interactions are pairwise. The grand resistance matrix in this case was derived by a pairwise summation of exact two-body solutions. The assumption of pairwise additivity should be accurate enough in the semi-dilute regime, so we will compare our present results with those former calculations.

Figure 5 shows effective translational and rotational dispersions under the conditions of $c = 0.1$, $\beta = 1$ and $G_{bh} = 0$. The solid and broken lines are the results of the former calculations using 27 squirmers assuming pairwise additivity; white and black circles are the present results using 64 squirmers. The function $y = bx$, where b is a constant, is drawn as a dotted line in the figure as well. We see that both results show similar dispersion coefficients and diverge from $y = bx$ at similar values of Δt. Both results agree well, which indicates that the interaction between squirmers in a semi-dilute regime can be correctly described by (2.18). We have also compared the rheological properties of a semi-dilute suspension of squirmers, and the results show good agreement, though they are omitted here.

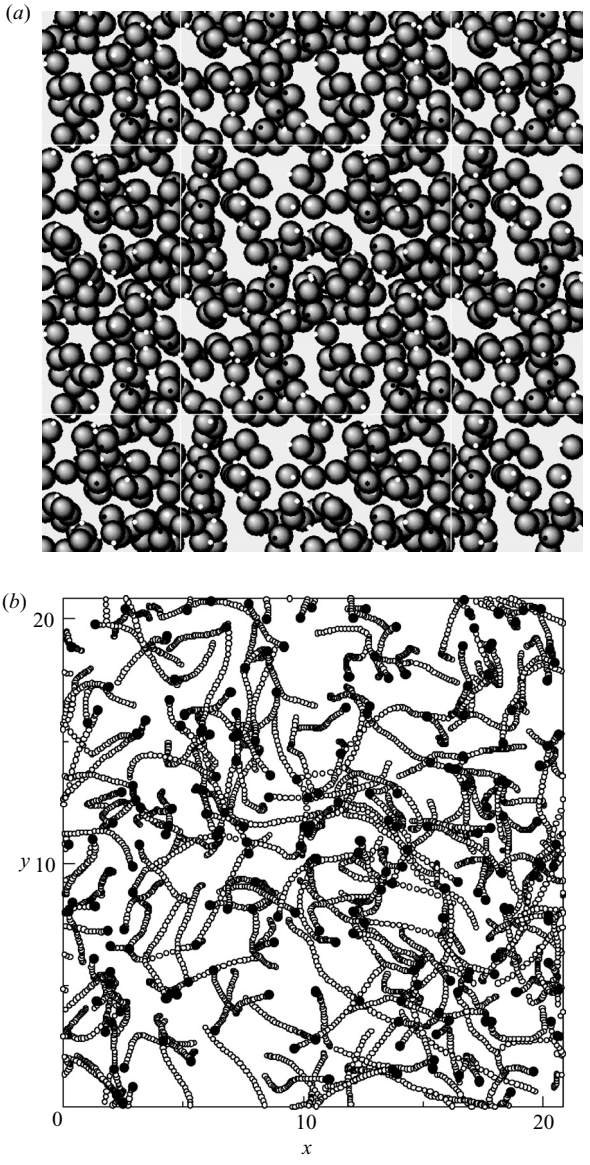

FIGURE 6. Distribution and trajectories of 216 squirmers with $\beta = 5$ and $c = 0.1$ ($G_{bh} = 0$). (a) Distribution of squirmers. Tops and bottoms of symmetry axes of squirmers are shown as white and black points respectively. The computational cell is located at the centre as indicated by the white lines. (b) Trajectories of squirmers. White circles are drawn from $t = 67$–70 with time intervals of 0.1. The positions of squirmers at $t = 70$ are drawn as black circles.

4. Coherent structures in suspensions of squirmers

Three-dimensional movement of non-bottom-heavy squirmers with $\beta = 5$ in a suspension with $c = 0.1$ is computed for random initial positions and orientations. The squirmer distribution at $t = 70$ in one realization is shown in figure 6(a), in which the front and back of the symmetry axis of a squirmer are drawn as white and black points, respectively. The computational cell is located at the centre of figure 6(a), and the region $-0.5H \leqslant x \leqslant 1.5H$, $-0.5H \leqslant y \leqslant 1.5H$, $0 \leqslant z \leqslant H$ is shown in the figure with the

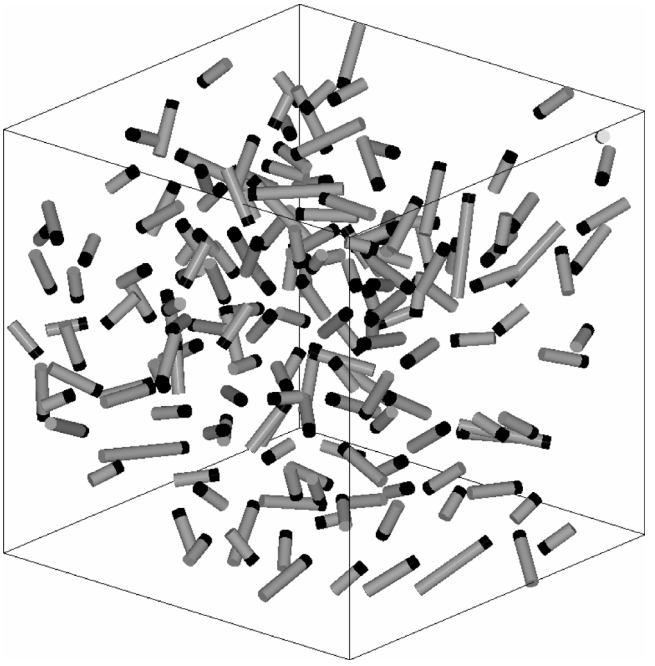

FIGURE 7. Velocities of squirmers with $\beta = 5$ and $c = 0.1$ ($G_{bh} = 0$). Only the velocities larger than 1 are shown as cylinders, in which the length of a cylinder is 1.5 times the absolute value of the velocity, and the centre position of the corresponding squirmer is expressed by a black tip. In some regions, neighbouring squirmers are swimming in similar directions.

z direction perpendicular to the figure. Figure 6(b) shows the trajectories of squirmers, in which a white circle is drawn for each squirmer at times $t = 67$ to $t = 70$ with a time interval of 0.1, and the positions of the squirmers at $t = 70$ are drawn as black circles. This figure shows only the computational cell, i.e. $0 \leqslant x, y, z \leqslant H$. We see that some squirmers appear to form a small cluster, and later we will calculate the radial distribution function to quantify the degree of aggregation. Note that by the time in the figure, $t = 70$, the system is already in statistical steady state, verified by the fact that the radial distribution function is time-independent for $t > 20$ (data not shown).

Figure 7 shows the squirmer velocities at $t = 70$, where only the velocities larger than 1 in the region $0 \leqslant x, y, z \leqslant H$ are shown as cylinders. The orientation of a cylinder corresponds to the direction of its velocity vector, and the origin of the velocity vector, i.e. the centre position of the corresponding squirmer, is expressed by a black tip. The length of a cylinder is 1.5 times the absolute value of the velocity. Cylinders are employed so that the three-dimensionality of velocity vectors in the figure becomes more apparent from the overlapping of three-dimensional objects. We see what appear to be collective motions. Dozens of squirmers locally move in similar directions, and the maximum velocity of a squirmer rises to about 3 in these simulations.

When c is as high as 0.4, the squirmers are quite closely packed, and we cannot clearly identify clusters, as shown in figure 8(a). The trajectories of squirmers are far from straight lines in this case, and squirmers interact considerably, as shown in figure 8(b). Figure 9 shows the squirmer velocities in a manner similar to figure 7; only the velocities larger than 1 in the region $0 \leqslant x, y, z \leqslant H$ are shown as cylinders, and the length of a cylinder is equal to the absolute value of the velocity. We again see some collective motions of squirmers, in which several squirmers swim in similar

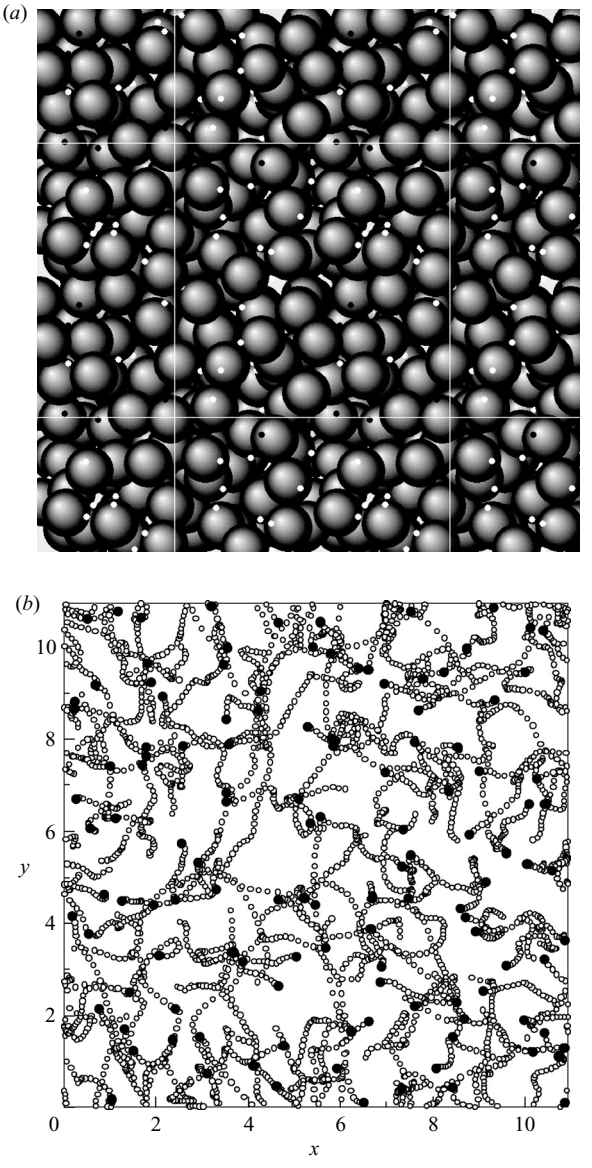

FIGURE 8. Distribution and trajectories of 216 squirmers with $\beta = 5$ and $c = 0.4$ ($G_{bh} = 0$). (a) Distribution of squirmers. Tops and bottoms of symmetry axes of squirmers are shown as white and black points respectively. The computational cell is located at the centre as indicated by the white lines. (b) Trajectories of squirmers. White circles are drawn from $t = 67$–70 with time intervals of 0.1. The positions of squirmers at $t = 70$ are drawn as black circles.

directions. The velocity of squirmers again rises to about 3 in these motions. The collective motions seen in figures 7 and 9 may be related to the 'slow turbulence' phenomenon observed by Dombrowski *et al.* (2004) or the mesoscale motion of whorls and jets observed by Mendelson *et al.* (1999), which will be discussed in § 6. Figures 6–9 suggest that suspensions of squirmers exhibit both aggregation and collective motions, and we will analyse these statistically in turn.

In order to quantify the degree of aggregation, we will calculate the radial distribution function $g(r)$ (McQuarrie 1976) and compare it to that for a hard-sphere

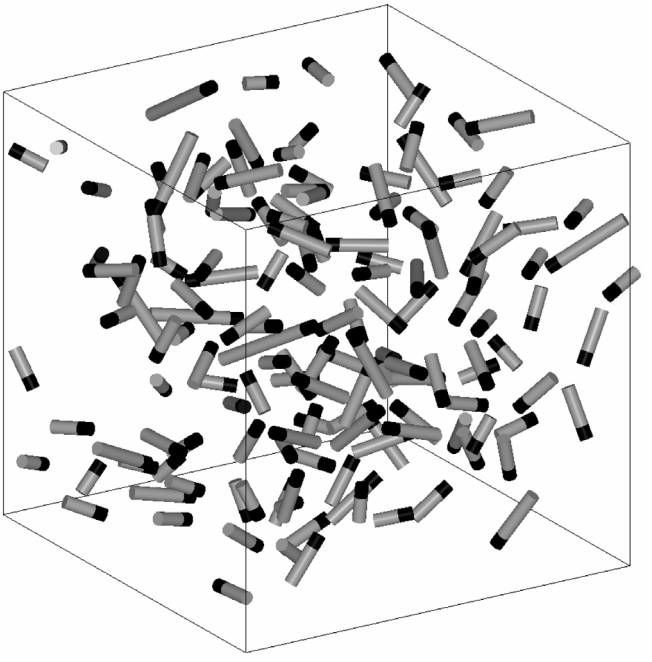

FIGURE 9. Velocities of squirmers $c = 0.4$ ($\beta = 5$ and $G_{bh} = 0$). Only the velocities larger than 1 are shown as cylinders, in which the length of a cylinder is the absolute value of the velocity, and the centre position of the corresponding squirmer is expressed by a black tip. In some regions, neighbouring squirmers are swimming in similar directions.

fluid. Mathematically, $\rho g(r) 4\pi r^2 \, \mathrm{d}r$, where ρ is the bulk number density of particles, is the average number of particles whose distance from a central particle is between r and $r + \mathrm{d}r$. An accurate formula for the hard-sphere fluid radial distribution function was reported by Trokhymchuk *et al.* (2005) over a range of volume fractions. Thus, we calculated the motion of 64 squirmers in a unit cell during $t = 0$–1500, and $g(r)$ was calculated by averaging between $t = 500$–1500. (It was necessary to wait until $t \approx 500$ to ensure that any ordered structure was well developed, at least for $c = 0.1$ and $\beta = 1$, as can be seen from figure 13.) Figure 10(*a*) shows $g(r)$ with various values of β and for $c = 0.1$. We see that $g(r)$ is significantly larger than the hard-sphere results for $r \leqslant 0.1$, which indicates that squirmers, such as those shown in figure 6, are more aggregated than particles in a hard-sphere fluid. The effect of β on $g(r)$ is not so strong, and we see similar tendencies for all values of β examined. Figure 10(*b*) shows $g(r)$ for $c = 0.4$. Relative to a particle in a hard-sphere fluid, a squirmer is more likely to have very close neighbours ($r < 2.03$) but less likely to have neighbours at intermediate distances ($2.03 < r < 2.8$). We see that $g(r)$ for $c = 0.4$ oscillates for large r and has a second peak around $r - 2 = 2$, for both the squirmer suspension and the hard-sphere fluid. This is caused by the second neighbouring sphere, which is often located at around $r = 4$ in a packed suspension. The effect of β on the $g(r)$ is not strong, as in the $c = 0.1$ case.

In order to clarify the scale of the collective motions seen in figures 7 and 9, we calculate the spatial correlation of squirmer velocities, defined as

$$I_U(r) = \frac{\langle \boldsymbol{U}(\boldsymbol{x}, t) \cdot \boldsymbol{U}(\boldsymbol{x} + \boldsymbol{r}, t) \rangle}{\langle \boldsymbol{U}^2(\boldsymbol{x}, t) \rangle}, \tag{4.1}$$

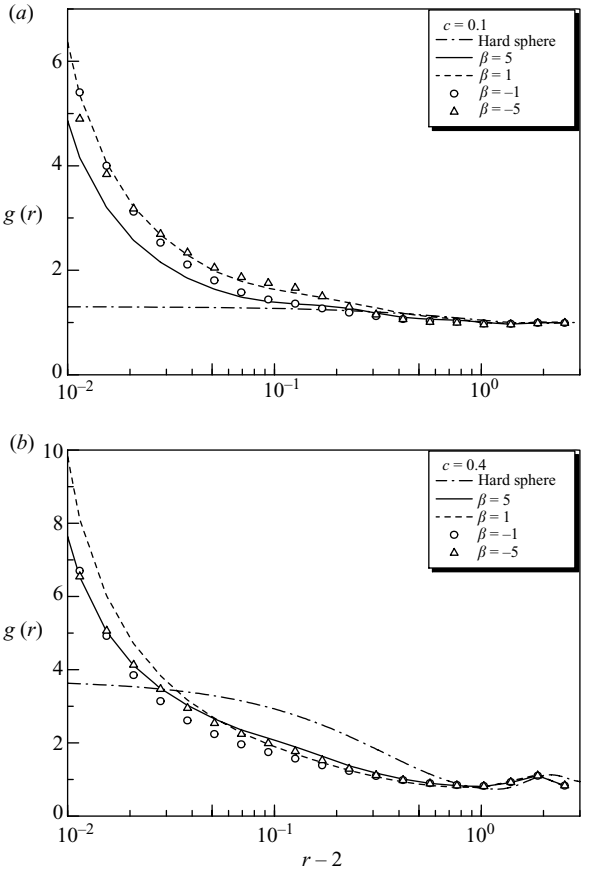

FIGURE 10. The effect of β on the radial distribution function $g(r)$ averaged between $t = 500$–1500 and ($N = 64$, $G_{bh} = 0$). The hard-sphere radial distribution function calculated analytically by Trokhymchuk *et al.* (2005) is indicated by *hard sphere*. (*a*) $c = 0.1$; (*b*) $c = 0.4$.

where r is the distance between squirmers. The brackets $\langle\rangle$ indicate an average value over N squirmers and over all different time steps after $t = 20$. $I_U(r)$ is defined only for $r \geqslant 2$, because two squirmers never come closer than $r = 2$. The results are shown in figures 11 and 12. The translational velocity correlation of $N = 216$ squirmers with $\beta = 5$ and $c = 0.1$ is shown in figure 11(*a*), where the results for $N = 125$ and 64 are also shown for comparison. I_U is positive when $r \leqslant 8$ and $N = 216$, so neighbouring squirmers tend to move together in a similar direction. Squirmers swimming together in a similar direction occupy the space of about $(4/3)\pi 8^3$, which is about 24 % of the total volume H^3. I_U shows anti-correlation when r is large, which is suggestive of a whirl structure. However, these results are strongly influenced by the size of the computational domain, because the whirl structure cannot be developed beyond it. Fortunately, however, the particle number does not qualitatively affect the results in the range used in this study, and we see similar collective motions of squirmers in all three cases. The translational velocity correlation of squirmers for $c = 0.4$ ($\beta = 5$) is shown in figure 11(*b*), where the results for $N = 125$ and 64 are also shown for comparison. The structure is similar to that of the $c = 0.1$ case.

The effect of the squirming parameter β, seen in (2.1), on the translational velocity correlation, averaged between $t = 500$–1500, is shown in figure 12. In these computations, we used a particle number $N = 640$, because it was necessary to

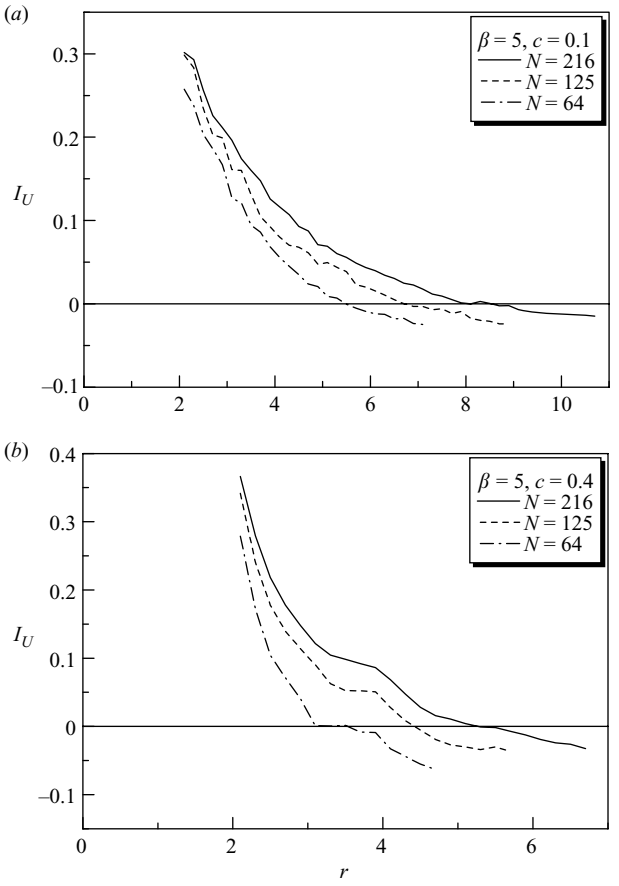

FIGURE 11. Correlation of the translational velocity of squirmers with $\beta = 5$ for $N = 64$, 125 and 216 ($G_{bh} = 0$). (*a*) $c = 0.1$ (Half of the computational cell size is about 10.4 for $N = 216$, 8.7 for $N = 125$ and 7 for $N = 64$.) (*b*) $c = 0.4$ (Half of the computational cell size is about 6.6 for $N = 216$, 5.5 for $N = 125$ and 4.4 for $N = 64$.)

compute for a very long time period, $t = 0$–1500, in order to identify ordered motions. We should note, however, that similar correlations also appear for $N = 27$ and $N = 100$, so the results shown here are qualitatively unaffected by the particle number. For $c = 0.1$ (figure 12*a*), I_U is positive in the whole region when $\beta = \pm 1$, indicating a globally ordered motion in which most squirmers move in approximately the same direction. I_U for $\beta = 1$ is larger than that for $\beta = -1$, so the squirmers with $\beta = 1$ show more ordered motion than those with $\beta = -1$. In the cases of $\beta = \pm 5$, on the other hand, I_U instead shows anti-correlation when $r > 5$ or 6, suggesting a whirl-like structure, though once again the limited computational domain means that we must be cautious in interpreting the results. For $c = 0.4$ (figure 12*b*), squirmers with $\beta = 1$ once again show a globally ordered motion (though the value of I_U is smaller than in the $c = 0.1$ case), but squirmers with $\beta = -1, \pm 5$ do not.

The squirmer velocity correlations apparent in $I_U(r)$ must ultimately be influenced by squirmer orientation correlations, so we calculate the spatial correlation of squirmer orientations, defined as $I_e(r) = \langle \boldsymbol{e}(\boldsymbol{x}) \cdot \boldsymbol{e}(\boldsymbol{x} + \boldsymbol{r}) \rangle$, where the brackets $\langle\rangle$ indicate an average value over squirmers and time steps. The results are shown in figure 13. We see that squirmers with $\beta = 1$ have correlated orientations even at large distances, for both $c = 0.1$ and $c = 0.4$. Squirmers with $\beta = -1$ have correlated orientations at long

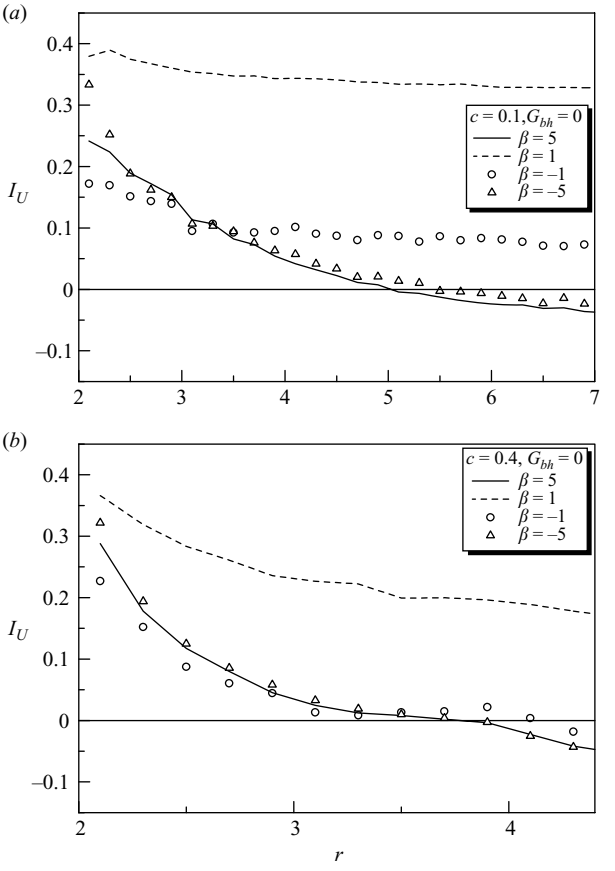

FIGURE 12. Effect of β on the correlation of translational velocity averaged between $t = 500$–1500 ($N = 64$, $G_{bh} = 0$). (*a*) $c = 0.1$ (Half of the computational cell size is about 7.) (*b*) $c = 0.4$ (Half of the computational cell size is about 4.4.)

distances for $c = 0.1$ but not for $c = 0.4$. Squirmers with $\beta = 5$ are weakly aligned at small distances, while squirmers with $\beta = -5$ are slightly anti-aligned at small distances. It is interesting to note that the squirmers' orientations are never anti-aligned at large distances even though their velocities are (cf. figures 11 and 12). The long-range order appearing for $\beta = \pm 1$ implies that the system is in a globally ordered state, what Toner, Tu & Ramaswamy (2005) called a 'ferromagnetic flock'. The reason why the ordered motion appears in the $\beta = 1$ case will be discussed in detail in § 5.

We also calculated the probability density of two squirmers having an angle θ between their orientation vectors and whose distance apart is between either 2 and 2.1 or 4 and 4.1. The results are shown in figure 14 ($\beta = 1$ and 5; $c = 0.1$ and 0.4), where the probability density is normalized so that it becomes unity when the orientation is isotropic at given distance r. We see that the peak of the probability density for $\beta = 1$ is around $\theta = 0$ even when $r = 4$, which again indicates that squirmers with $\beta = 1$ tend to have similar orientation in these simulations.

Since, for some values of β, the squirmers' orientations are ordered across the whole simulation domain, it makes sense to quantify this global orientational order via the squirmer-averaged orientation vector, defined as

$$\boldsymbol{e}_{mean} = \frac{1}{N} \sum_{i=1}^{N} \boldsymbol{e}_i. \tag{4.2}$$

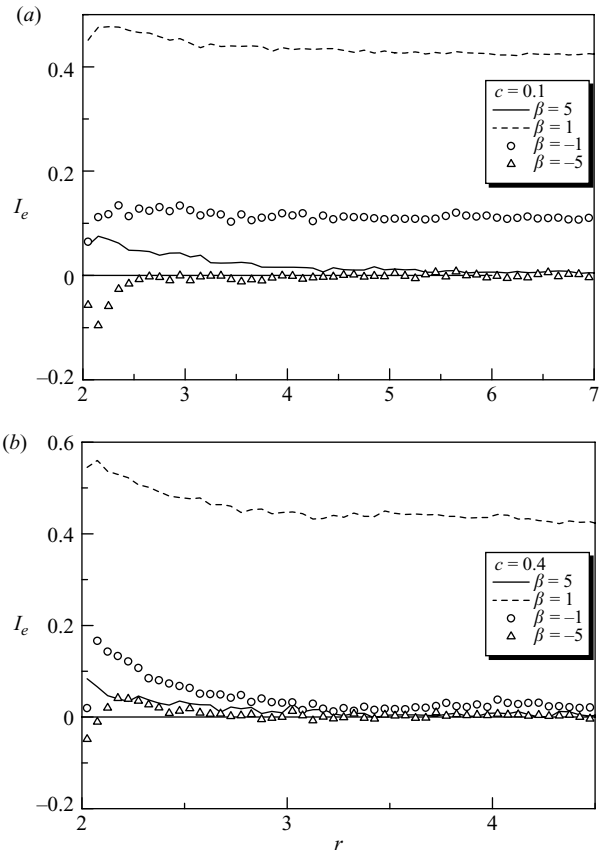

FIGURE 13. The spatial correlation of the orientation of the squirmers for different values of c and β (averaged between $t = 500$–1500 with $N = 64$). (*a*) $c = 0.1$ (Half of the computational cell size is about 7.) (*b*) $c = 0.4$ (Half of the computational cell size is about 4.4.)

Now $|\boldsymbol{e}_{mean}|$ is an 'order parameter' for the system, since $|\boldsymbol{e}_{mean}| = 1$ if all the squirmers face in the same direction, and one can show that $|\boldsymbol{e}_{mean}| \approx 1/\sqrt{N}$ if the squirmers face isotropically random directions. Figure 15 shows the time dependence of $|\boldsymbol{e}_{mean}|$ for $c = 0.1$ and various values of β, with $N = 64$. (The calculation was repeated with $N = 27$ and $N = 100$, and the results were qualitatively unchanged.) For $\beta = \pm 1$, $|\boldsymbol{e}_{mean}|$ grows initially and then saturates at a value $\gg 1/\sqrt{N}$, indicating a globally ordered suspension in which most squirmers swim in a similar direction. The time until saturation is approximately 300 time units. After saturation, the group swimming direction (i.e. the direction of $\boldsymbol{e}_{mean}$) drifts slowly over time, on a time scale of 100 s (data not shown). This is the reason why we think that the ordered motion is stable for the time scale of 100 time units. For $\beta = \pm 5$, however, $|\boldsymbol{e}_{mean}|$ remains $\approx 1/\sqrt{N}$, indicating an absence of global order. Figure 15(*b*) shows the same statistics, now computed for a higher volume fraction of $c = 0.4$. The $\beta = 1$ case again shows significant global order ($|\boldsymbol{e}_{mean}| \approx 0.7 \gg 1/\sqrt{N}$), and the time until saturation is shorter, around 100 time units. The $\beta = -1$ case no longer shows global order, and the $\beta = \pm 5$ cases also show no global order ($|\boldsymbol{e}_{mean}| \approx 1/\sqrt{N}$).

G_{bh} is the ratio of the gravitational torque to a scale for the viscous torque, defined by (2.21). If one assume that micro-organisms swim in water at 5 body lengths per second with their centre of mass $0.2a$ down from the geometric centre (as is roughly

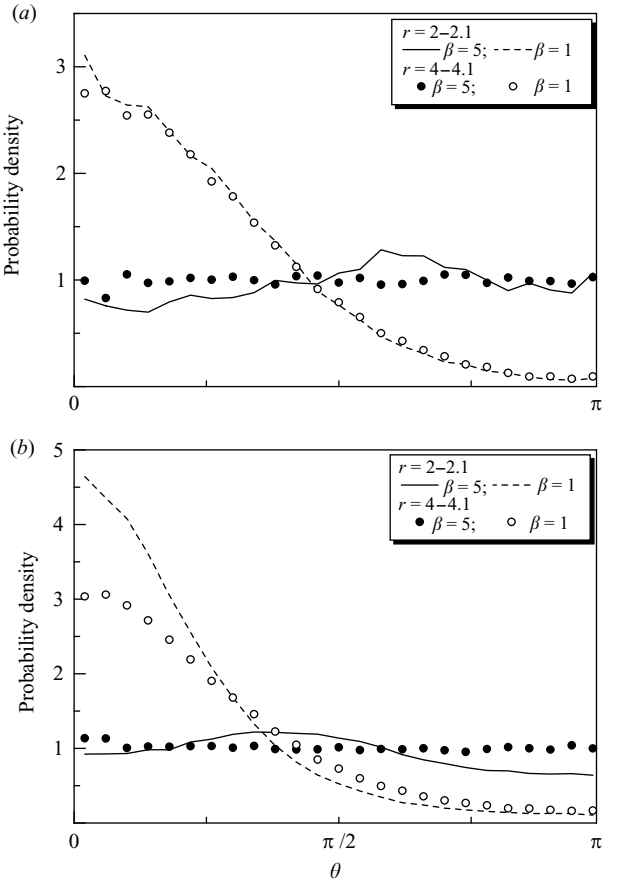

FIGURE 14. The probability density of two squirmers having an angle θ between their orientation vectors and whose distance apart is between either 2 and 2.1 or 4 and 4.1 for different values of c and β (averaged between $t = 500$–1500 with $N = 64$). (*a*) $c = 0.1$; (*b*) $c = 0.4$.

the case for *Chlamydomonas nivalis*; Kessler 1986), G_{bh} is about 100 for micro-organisms with radii of 125 μm. The trajectories of bottom-heavy squirmers with $G_{bh} = 100$ and $\beta = 5$ are shown in figure 16; the gravitational direction is downwards. The squirmers clearly tend to swim upwards, but the trajectories are far from straight lines, and the effect of hydrodynamic interaction is very strong when $\beta = 5$ even with $G_{bh} = 100$. Figure 17 shows the squirmer velocities relative to the average velocity of squirmers, where only the velocities larger than 0.5 in $0 \leqslant x, y, z \leqslant H$ are shown as cylinders, and the length of a cylinder is the absolute value of the velocity. We see some collective motions for bottom-heavy squirmers, which are mainly in the vertical direction. We also performed simulations of bottom-heavy squirmers with various β values. The results show that squirmers tend to swim upwards more smoothly as the absolute value of β is decreased, though the results are omitted here.

5. Statistics of near-field interactions

A question of interest is whether the ordered motions seen in the $\beta = 1$ simulations are due to near-field or far-field interactions. On the one hand, the far-field velocity

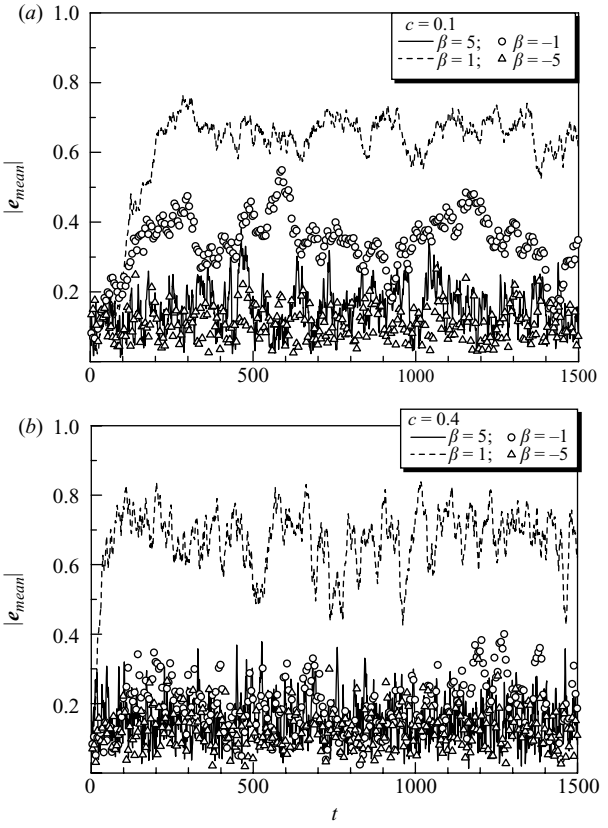

FIGURE 15. Time dependence of the magnitude of the squirmer-averaged swimming direction for different values of c and β (averaged between $t = 500$–1500 with $N = 64$). An $|\boldsymbol{e}_{mean}|$ close to 1 indicates that all the squirmers are swimming in a common direction. (*a*) $c = 0.1$; (*b*) $c = 0.4$.

of an individual squirmer decays like r^{-2}, and this slow decay suggests that there may be strong far-field interactions. On the other hand, the aggregation of squirmers demonstrated in figure 10 suggests that near-field interactions play an important role. By calculating certain statistics, we can demonstrate that it is in fact the near-field interactions that are responsible for the ordered motion.

One way of showing that near-field interactions are responsible for alignment in the $\beta = 1$ simulations is to look at the rate of change of the alignment between a squirmer and the squirmer-averaged swimming direction, as a function of the distance between a squirmer and its nearest neighbour. The quantity $\boldsymbol{e} \cdot \boldsymbol{e}_{mean}$ is a measure of the alignment between a squirmer and the squirmer-averaged swimming direction, and the rate of change of this alignment is $(\mathrm{d}/\mathrm{d}t)(\boldsymbol{e} \cdot \boldsymbol{e}_{mean})$. For convenience, let us define $\eta(d)$ as the expectation of $(\mathrm{d}/\mathrm{d}t)(\boldsymbol{e} \cdot \boldsymbol{e}_{mean})$, where the expectation is taken by averaging over all instances in which the squirmer is a distance d from its nearest neighbour. Symbolically,

$$\eta(d) = \left\langle \frac{\mathrm{d}}{\mathrm{d}t}(\boldsymbol{e} \cdot \boldsymbol{e}_{mean}) \right\rangle_{\text{n.n.dist}=d}, \tag{5.1}$$

where 'n.n.dist $= d$' indicates that the nearest neighbour distance equals d. Also, let $p(d)$ denote the probability density function for the distance d between a squirmer

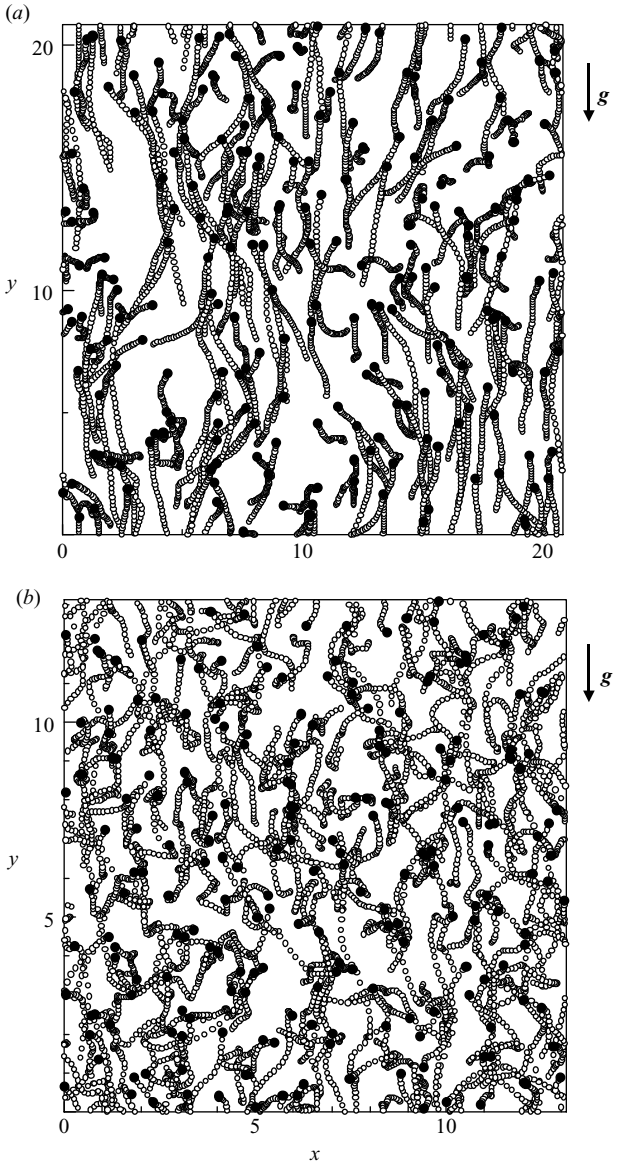

FIGURE 16. Trajectories of 216 bottom-heavy squirmers with $G_{bh} = 100$ and $\beta = 5$. (White circle is drawn from $t = 67$–70 with a time interval of 0.1. The position of squirmers at $t = 70$ is drawn as a black circle.) The gravitational direction is downwards as shown in the figure. (*a*) $c = 0.1$; (*b*) $c = 0.4$.

and its nearest neighbour. Figure 18 shows a plot of $\eta(d)p(d)$ versus d. It clearly shows that a squirmer tends to align with the squirmer-averaged swimming direction when it is very close to a neighbour and lose alignment with the squirmer-averaged swimming direction when it is not close to a neighbour. The plot does not capture the true height of the leftmost peak because of the finite histogram bin width; in reality the peak is narrower and higher. The plot was calculated using a subset of the simulation data over which the system was in statistical steady state, i.e. leaving out the early time data in which the order parameter $|\boldsymbol{e}_{mean}|$ was still rising (cf. figure 15).

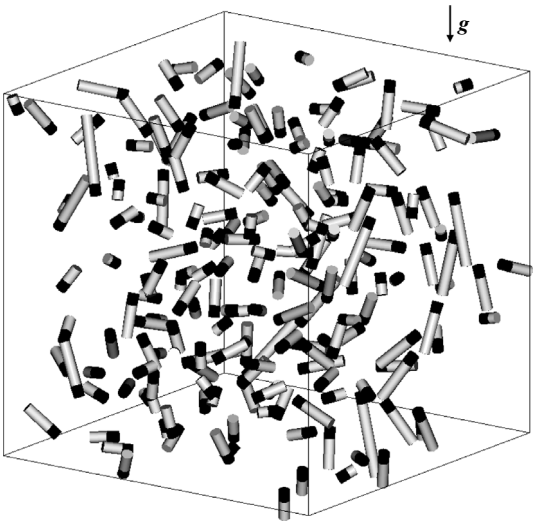

FIGURE 17. Velocities of 216 squirmers relative to the average velocity in the three-dimensional configuration with $c = 0.4$ ($\beta = 5$ and $G_{bh} = 100$). Only the velocities larger than 0.5 are shown as cylinders, in which the length of a cylinder is the absolute value of the velocity, and the centre position of the corresponding squirmer is expressed by a black tip. Some collective motions appear, mainly in the vertical direction.

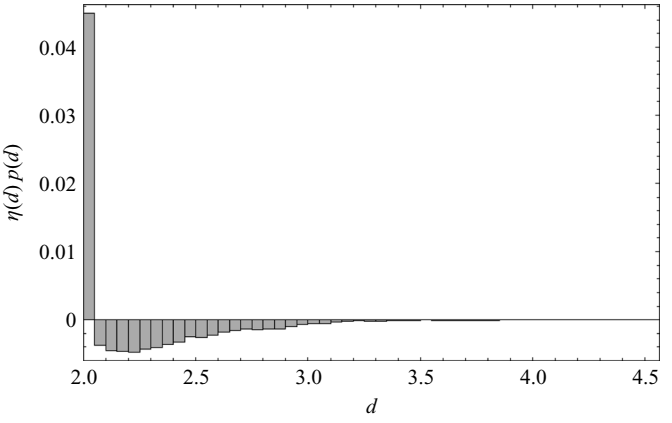

FIGURE 18. Approximate rate of change η of the alignment between a squirmer and the squirmer-averaged swimming direction, as a function of the distance d between the squirmer and its nearest neighbour, and weighted by the probability density p of the nearest neighbour distance, for a simulation with $\beta = 1$, $c = 0.1$ and $N = 64$.

Another way of showing that near-field interactions are responsible for alignment in the $\beta = 1$ simulations is to analyse those intervals of time in which a squirmer is close to a neighbour. Let us define a 'near interval' as an interval of time in which the distance between a particular squirmer i and its nearest neighbour k is less than some cutoff distance d_{cut}. We choose $d_{\mathrm{cut}} = 2.1$, but the results are qualitatively unchanged for other choices of d_{cut}. Collating the results from many near intervals, we calculate the distributions of $\boldsymbol{e}_i \cdot \boldsymbol{e}_k$ at the beginning and end of near intervals; the results are shown in figure 19. For the case $\beta = 1$, $c = 0.1$, $N = 64$, the mean value of $\boldsymbol{e}_i \cdot \boldsymbol{e}_k$ increases from 0.22 to 0.34 over the near interval, indicating that two neighbouring

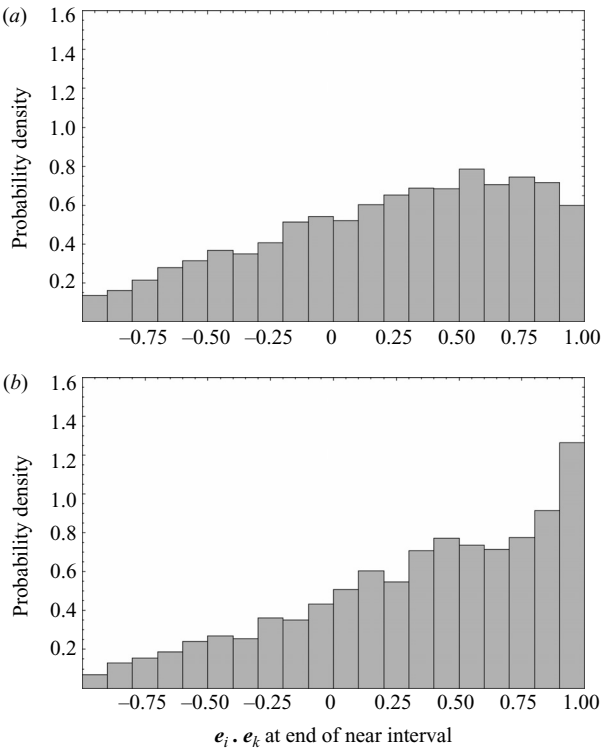

FIGURE 19. Approximate probability density function for the dot product $\boldsymbol{e}_i \cdot \boldsymbol{e}_k$ of nearest neighbour swimming directions at the beginning or end of near intervals for a simulation with $\beta = 1$, $c = 0.1$ and $N = 64$. (*a*) At the beginning of near intervals, where the mean value of $\boldsymbol{e}_i \cdot \boldsymbol{e}_k$ is 0.22. (*b*) At the end of near intervals, where the mean value of $\boldsymbol{e}_i \cdot \boldsymbol{e}_k$ is 0.34.

squirmers are significantly more aligned after a near-field interaction than before. Figure 19(*b*) can also be thought of as showing the histogram at the start of a 'not-near interval', with figure 19(*a*) showing it at the end: clearly the alignment decreases when the squirmers are not very close together. Thus, it is the near-field interactions that are responsible for the ordered behaviour.

Examination of near intervals also yields some insight into why the $\beta = 5$ simulations exhibit less ordered behaviour. For $\beta = 5$, the near intervals have a less aligning effect. The mean value of $\boldsymbol{e}_i \cdot \boldsymbol{e}_k$ increases only very slightly from ≈ 0 to 0.04 over a near interval for simulations with $\beta = 5$, $c = 0.1$, $N = 216$ (distributions not shown). In the case in which the volume concentration c is 0.4, the distance between a squirmer and its nearest neighbour is almost always less than 2.1, so squirmers are constantly interacting with one another by near-field interactions, and one cannot break a squirmer's trajectory into a series of discrete near intervals.

In the present study, both lubrication forces and repulsive forces are generated when two squirmers are very near to contact ($r - 2 \leqslant 0.001$). In order to separate the effect of these two forces, we performed a similar simulation as for figure 13(*a*) ($c = 0.1$, $\beta = 1$, $N = 64$) but without the lubrication forces. The grand resistance matrix in this case is just $\boldsymbol{R}^{far}$. To avoid the very small time step needed to prevent the overlapping of particles, the coefficients of the repulsive force given by (2.20) are set as $\alpha_1 = 1$, $\alpha_2 = 20$. The same repulsive force is used in the simulation with the lubrication forces for comparison. The spatial correlation of the orientation of the

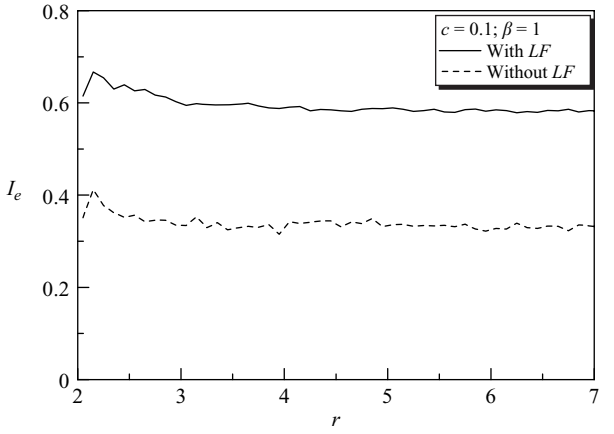

FIGURE 20. The effect of lubrication forces on the spatial correlation of the orientation of the squirmers ($c = 0.1$, $\beta = 1$ and $N = 64$). The coefficients for the lubrication force are $\alpha_1 = 1$ and $\alpha_2 = 20$. The inclusion of the near-field lubrication forces in constructing the grand resistance matrix is indicated by with LF, whereas without LF indicates that they are not included.

squirmers defined by $\langle \boldsymbol{e}(0) \cdot \boldsymbol{e}(r) \rangle$, with or without the lubrication forces, are shown in figure 20. We see that the spatial correlation falls considerably if the lubrication forces are neglected. These results also support the proposal that the near-field hydrodynamics play an important role in generating the coherent structures. The physical mechanism underlying the alignment of neighbouring squirmers is still under investigation.

6. Discussion

The main conclusions of this work are that, for a suspension of self-propelled spherical squirmers, (*a*) coherent structures, such as aggregation and collective motions, can emerge from purely hydrodynamic interactions; and (*b*) in principle, details of the near field have a strong impact on the formation of coherent structures. Although most micro-organisms do not resemble squirmers, we believe that these conclusions will remain true for real micro-organism suspensions.

We now investigate whether the current numerical results can be usefully compared with previous experimental, analytical and computational findings. The previous studies considered are (*a*) slow turbulence caused by the collective motion of *B. subtilis* (Dombrowski *et al.* 2004), (*b*) patterns of whirls and jets observed in *B. subtilis* colonies (Mendelson *et al.* 1999; Lega & Passot 2003) and (*c*) numerical models for systems of self-driven particles (Vicsek *et al.* 1995; Hernandes-Ortiz *et al.* 2005; Saintillan & Shelley 2007).

Dombrowski *et al.* (2004) have reported a collective motion of bacteria in a sessile drop of *B. subtilis* suspension, where *B. subtilis* is a rod-shaped bacterium with aspect ratio of about 6. (The cell concentration is not mentioned in the paper.) The cells tend to swim in the same direction as their neighbours, generating a mesoscale coherent structure in the flow. The mesoscale structure, called slow turbulence, changes its direction randomly in a manner reminiscent of real turbulence. Some of the collective motions observed in this study, such as figures 7 and 9, have a similar structure, too. Dombrowski *et al.* investigated the velocity correlation, analogous to (4.1), and

the anti-correlation appears around $50\,\mu\mathrm{m} < r$ in their experiment. They observed the cell motions from the bottom of a petri dish, so the motions were restricted by a wall. By assuming that the typical body length of *B. subtilis* is about $4\,\mu\mathrm{m}$, the value $50\,\mu\mathrm{m} < r$ corresponds to $12.5 < r$ in dimensionless form, which is greater than the present result of 5–8 (see figure 11). The quantitative difference may be caused by the limited computational cell size employed in this study. In future studies, we would like to clarify this by using a much larger computational cell size, containing many more squirmers.

Organized cell swimming motions in *B. subtilis* colonies were reported by Mendelson *et al.* (1999). They observed a mesoscale motion in a water film above an agar gel, so the organized motions are restricted to a two-dimensional plane. (The cell concentration is not mentioned in the paper.) In their experiments, individual cells swam at rates between 76 and $116\,\mu\mathrm{m\,s^{-1}}$ and were organized into patterns of whirls, each approximately $1000\,\mu\mathrm{m}^2$, and jets of about $95 \times 12\,\mu\mathrm{m}$. Whirls and jets were short-lived, lasting only about 0.25 s. By assuming that the typical body length of *B. subtilis* is $4\,\mu\mathrm{m}$ and that it swims at a speed of $96\,\mu\mathrm{m\,s^{-1}}$, all dimensional values mentioned above can be non-dimensionalized. The size of a typical whirl is approximately 8×8, and that of a jet is about 24×3. Although cell swimming motions in a fully three-dimensional domain are analysed in the present study, instead of that in a two-dimensional film, the length scale of each whirl appearing in the present study is rather similar to the structures found in the experiment, which is about 5–8. Some of the collective motions observed in this study, figures 7 and 9 for instance, may be similar to the jet structure, though the definition of the jet is unclear. The whirls and jets in the experiments last for about 6 dimensionless time units. The time scale of the whirl structure in the present study is also about 6–8. (The time scale is calculated by calculating velocity correlations in time, analogous to (4.1), though the figure is omitted in this paper.) Although the length and time scales in the experiment and present study are similar, we need further investigations to check them in a much larger computational cell.

In a previous study, we investigated coherent structures in monolayers of squirmers, i.e. in a two-dimensional suspension (Ishikawa & Pedley 2008). The squirmers in a monolayer also generated whirl structures, when the areal fraction of squirmers was higher than 0.3 and when $\beta = 5$. The length scale of each whirl was about 8. Thus, the length scale of a typical whirl is not much different between two and three dimensions. However, we observed aggregation of squirmers much more clearly in a monolayer, when the areal fraction of squirmers was small. So the coherent structures in two and three dimensions are considerably different (Ishikawa & Pedley 2008). Another study of self-propelled spheres in a two-dimensional simulation has been reported by Mehandia & Nott (2007), with similar conclusions about aggregation.

Vicsek *et al.* (1995) proposed a simple numerical model for the analysis of self-ordered motions in systems of particles that experience some sort of biological interaction. In their model particles are driven with a constant speed on a two-dimensional plane and at each time step assume the average direction of motion of the particles in their neighbourhood with some random perturbation added. Though this is a simple model, it results in collective motions similar to those observed in this study. In Vicsek's model, when the areal fraction of particles is large and the random perturbations are small, the particles tend to swim in the same direction. This behaviour is similar to that found here for non-bottom-heavy squirmers with $\beta = \pm 1$, at least at lower volume fraction ($c = 0.1$; cf. figures 12 and

13). When areal fraction and random perturbations are both large, in Vicsek's model, the particles move randomly with some correlation. This behaviour is similar to that for $\beta = 5$, as shown in figures 7 and 9. Our squirmer model has no random perturbation (except in initial condition), but the similarities in the results suggest that the hydrodynamic interactions are analogous to random perturbations, and more vigorous squirming ($|\beta| = 5$ as opposed to $|\beta| = 1$) gives rise to larger random perturbations. This viewpoint is consistent with that proposed in our earlier study of self-diffusion in a semi-dilute suspension of squirmers (Ishikawa & Pedley 2007*b*). However, as opposed to Vicsek's model, we observe that in some cases a higher number density can reduce the order in the system (cf. figure 15; $\beta = 1$).

Lega & Passot (2003) used a two-dimensional continuum model to analyse the evolution of bacterial colonies growing on soft agar plates. Their simulations also gave rise to various colony patterns as well as whirl structures in the colonies. However, the hydrodynamics around individual cells were not analysed, and an *ad hoc* random-body force was employed to represent sub-grid scale dynamics. In order to understand the mechanism of organized cell swimming motion, we believe that it is important to model individual cells and solve for their collective motion as a result of interaction between individuals, without making any *ad hoc* assumption for individual cells.

Recently, Hernandes-Ortiz *et al.* (2005) performed direct simulations of large populations of confined hydrodynamically interacting swimming particles. The computational cell size they employed was much larger than the observed coherent structures, and they showed that hydrodynamic coupling between the swimmers led to coherent vortex motions in the flow, which had a scale larger than individual swimmers and comparable to the depth of the simulation box. Although their simulation methods allowed them to deal with a much larger computational system than the present study, they did not treat near-field fluid dynamics precisely. A swimming bacterium was modelled as two rigidly linked beads which exert equal and opposite point forces on the fluid. The structure moves and rotates in response to the low-Reynolds-number flow of the suspending medium, driven by all the other structures. Using point forces or point stresslets is good enough to model the far-field interactions between particles, because higher moments decay rapidly in the far field. In considering near-field interactions, however, one cannot describe the lubrication flow in terms of a few point singularities. Most recently Saintillan & Shelley (2007) used slender-body theory to investigate orientational order in suspensions of self-locomoting rods. A bacterium is modelled as a slender rod-like particle, which propels itself by exerting an axisymmetric tangential shear stress on the fluid over a section of its body, while the remainder of its body is subject to the usual no-slip boundary condition (a sort of ellipsoidal squirmer). Hydrodynamic interactions were captured through the disturbance velocity, which is the fluid velocity induced by the force distributions. Though their simulation methods could also deal with a much larger computational systems than the present study, they again did not treat near-field hydrodynamics precisely. In the present study, we solve both far- and near-field interactions precisely and perform Brady's Stokesian dynamics simulation of squirmers for the first time to our knowledge.

The authors are grateful for helpful discussions to Professor E. J. Hinch and Professor J. M. Rallison in Department of Applied Mathematics and Theoretical Physics, University of Cambridge. This work was partly supported by Grant-in-Aid for Young Scientists (A) by the Japan Society for the Promotion of Science.

REFERENCES

Acrivos, A. 1995 Bingham award lecture 1994: shear-induced particle diffusion in concentrated suspension of noncolloidal particles. *J. Rheol.* **39**, 813–825.

Batchelor, G. K. 1970 The stress system in a suspension of force-free particles. *J. Fluid Mech.* **41**, 545–570.

Beenakker, C. W. J. 1986 Ewald sum of the Rotne–Prager tensor. *J. Chem. Phys.* **85**, 1581–1582.

Bees, M. A. & Hill, N. A. 1998 Linear bioconvection in a suspension of randomly-swimming, gyrotactic micro-organisms. *Phys. Fluids* **10**, 1864–1881.

Blake, J. R. 1971 A spherical envelope approach to ciliary propulsion. *J. Fluid Mech.* **46**, 199–208.

Brady, J. F. & Bossis, G. 1985 The rheology of concentrated suspensions of spheres in simple shear flow by numerical simulation. *J. Fluid Mech.* **155**, 105–129.

Brady, J. F. & Bossis, G. 1988 Stokesian dynamics. *Annu. Rev. Fluid Mech.* **20**, 111–157.

Brady, J. F. & Morris, J. F. 1997 Microstructure of strongly sheared suspensions and its impact on rheology and diffusion. *J. Fluid Mech.* **348**, 103–139.

Brady, J. F., Phillips, R. J., Lester, J. C. & Bossis, G. 1988 Dynamic simulation of hydrodynamically interacting suspensions. *J. Fluid Mech.* **195**, 257–280.

Childress, S., Levandowsky, M. & Spiegel, E. A. 1975 Pattern formation in a suspension of swimming micro-organisms: equations and stability theory. *J. Fluid Mech.* **63**, 591–613.

Dombrowski, C., Cisneros, L., Chatkaew, S., Goldstein, R. E. & Kessler, J. O. 2004 Self-Concentration and large-scale coherence in bacterial dynamics. *Phys. Rev. Lett.* **93**, 098103.

Durlofsky, L., Brady, J. F. & Bossis, G. 1987 Dynamic simulation of hydrodynamically interacting particles. *J. Fluid Mech.* **180**, 21–49.

Felderhof, B. U. & Jones, R. B. 2004 Small-amplitude swimming of a sphere. *Physica* A **202**, 119–144.

Guell, D. C., Brenner, H., Frankel, R. B. & Hartman, H. 1988 Hydrodynamic forces and band formation in swimming magnetotactic bacteria. *J. Theor. Biol.* **135**, 525–542.

Hernandes-Ortiz, J. P., Stoltz, C. G. & Graham M. D. 2005 Transport and collective dynamics in suspensions of confined swimming particles. *Phys. Rev. Lett.* **95**, 204501.

Hillesdon, A. J., Pedley, T. J. & Kessler, J. O. 1995 The development of concentration gradients in a suspension of chemotactic bacteria. *Bull. Math. Biol.* **57**, 299–344.

Ishikawa, T. & Hota, M. 2006 Interaction of two swimming *Paramecia*. *J. Exp. Biol.* **209**, 4452–4463.

Ishikawa, T. & Pedley, T. J. 2007*a* The rheology of a semi-dilute suspension of swimming model micro-organisms. *J. Fluid Mech.* **588**, 399–435.

Ishikawa, T. & Pedley, T. J. 2007*b* Diffusion of swimming model micro-organisms in a semi-dilute suspension. *J. Fluid Mech.* **588**, 437–462.

Ishikawa, T. & Pedley, T. J. 2008 Coherent structures in monolayers of swimming particles. *Phys. Rev. Lett.* **100**, 088103.

Ishikawa, T., Sekiya, G., Imai, Y. & Yamaguchi, T. 2007 Hydrodynamic interaction between two swimming bacteria. *Biophys. J.* **93**, 2217–2225.

Ishikawa, T., Simmonds, M. P. & Pedley, T. J. 2006 Hydrodynamic interaction of two swimming model micro-organisms. *J. Fluid Mech.* **568**, 119–160.

Jiang, H., Osborn, T. R. & Meneveau, C. 2002 Hydrodynamic interaction between two copepods: a numerical study. *J. Plank. Res.* **24**, 235–253.

Kessler, J. O. 1986 The external dynamics of swimming micro-organisms. In *Progress in Phycological Research* (ed. F. E. Round & D. J. Chapman; vol. 4), pp. 257–307. Bristol: Biopress.

Kessler, J. O., Hoelzer, M. A., Pedley, T. J. & Hill, N. A. 1994 Functional pattern of swimming bacteria. In *Mechanics and Physiology of Animal Swimming* (ed. L. Maddock, Q. Bone & J. M. V. Rayner), pp. 3–12. Cambridge University Press.

Kim, S. & Karrila, S. J. 1992 *Microhydrodynamics: Principles and Selected Applications*. Butterworth Heinemann.

Ladd, A. J. C. 1994*a* Numerical simulations of particlate suspensions via a discretized Boltzmann equation: part 1; theoretical foundation. *J. Fluid Mech.* **271**, 285–309.

Ladd, A. J. C. 1994*b* Numerical simulations of particlate suspensions via a discretized Boltzmann equation: part 2; numerical results. *J. Fluid Mech.* **271**, 311–339.

Ladd, A. J. C. 1997 Sedimentation of homogeneous suspensions of non-Brownian spheres. *Phys. Fluids* **9**, 491–499.

Lega, J. & Passot, T. 2003 Hydrodynamics of bacterial colonies. *Phys. Rev.* E **67**, 031906.

Lighthill, M. J. 1952 On the squirming motion of nearly spherical deformable bodies through liquids at very small Reynolds numbers. *Comm. Pure Appl. Maths* **5**, 109–118.

Loewenberg, M. & Hinch, E. J. 1996 Numerical simulations of a concentrated emulsion in shear flow. *J. Fluid Mech.* **321**, 395–419.

Magar, V., Goto, T. & Pedley, T. J. 2003 Nutrient uptake by a self-propelled steady squirmer. *Q. J. Mech. Appl. Maths* **56**, 65–91.

Magar, V. & Pedley, T. J. 2005 Average nutrient uptake by a self-propelled unsteady squirmer. *J. Fluid Mech.* **539**, 93–112.

McQuarrie, D. A. 1976 *Statistical Mechanics* (Harper's chemistry series). Harper and Row.

Mehandia, V. & Nott, P. 2007 The collective dynamics of self-propelled particles. *J. Fluid Mech.* **595**, 239–264.

Mendelson, N. H., Bourque, A., Wilkening, K., Anderson, K. R. & Watkins, J. C. 1999 Organised cell swimming motions in *Bacillus subtilis* colonies: patterns of short-lived whirls and jets. *J. Bacteriol.* **180**, 600–609.

Metcalfe, A. M. & Pedley, T. J. 2001 Falling plumes in bacterial bioconvection. *J. Fluid Mech.* **445**, 121–149.

Nasseri, S. & Phan-Thien, N. 1997 Hydrodynamic interaction between two nearby swimming micromachines. *Comp. Mech.* **20**, 551–559.

Nunan, K. C. & Keller, J. B. 1984 Effective viscosity of a periodic suspension. *J. Fluid Mech.* **142**, 269–287.

Pedley, T. J. & Kessler, J. O. 1990 A new continuum model for suspensions of gyrotactic micro-organisms. *J. Fluid Mech.* **212**, 155–182.

Pitta, T. P. & Berg, H. C. 1995 Self-electrophoresis is not the mechanism for motility in swimming cynobacteria. *J. Bacteriol.* **177**, 5701–5703.

Pozrikidis C. 1992 *Boundary Integral and Singularity Methods for Linearized Viscous Flow*, chapter 4. Cambridge University Press.

Ramia, M., Tullock, D. L. & Phan-Thien, N. 1993 The role of hydrodynamic interaction in the locomotion of microorganisms. *Biophys. J.* **65**, 755–778.

Saintillan, D. & Shelley, M. J. 2007 Orientational order and instabilities in suspensions of self-locomoting rods. *Phys. Rev. Lett.* **99**, 058102.

Sangani, A. S. & Mo, G. 1996 An O(N) algorithm for Stokes and Laplace interactions of particles. *Phys. Fluids* **8**, 1990–2010.

Stone, H. A. & Samuel, A. D. T. 1996 Propulsion of microorganisms by surface distortions. *Phys. Rev. Lett.* A **77**, 4102–4104.

Toner, J., Tu, Y. & Ramaswamy, S. 2005 Hydrodynamics and phases of flocks. *Ann. Phys.* A **318**, 170–244.

Trokhymchuk, A., Nezbeda, I., Jirsák, J. & Henderson D. Hard-sphere radial distribution function again. *J. Chem. Phys.* **123**, 024501–024510.

Vicsek, T., Czirók, A., Ben-Jacob, E., Cohen, I. & Shochet, O. 1995 Novel type of phase transition in a system of seif-driven particles. *Phys. Rev. Lett.* **75**, 1226–1229.

Waterbury, J. B., Willey, J. M., Franks, D. G., Valois, F. W. & Watson, S. W. 1985 A cyanobacterium capable of swimming motility. *Science* **230**, 74–76.

Zinchenko, A. Z. & Davis, R. H. 2000 An efficient algorithm for hydrodynamical interaction of many deformable drops. *J. Comp. Phys.* **157**, 539–587.

Zinchenko, A. Z. & Davis, R. H. 2002 Shear flow of highly concentrated emulsions of deformable drops by numerical simulations. *J. Fluid Mech.* **455**, 21–62.